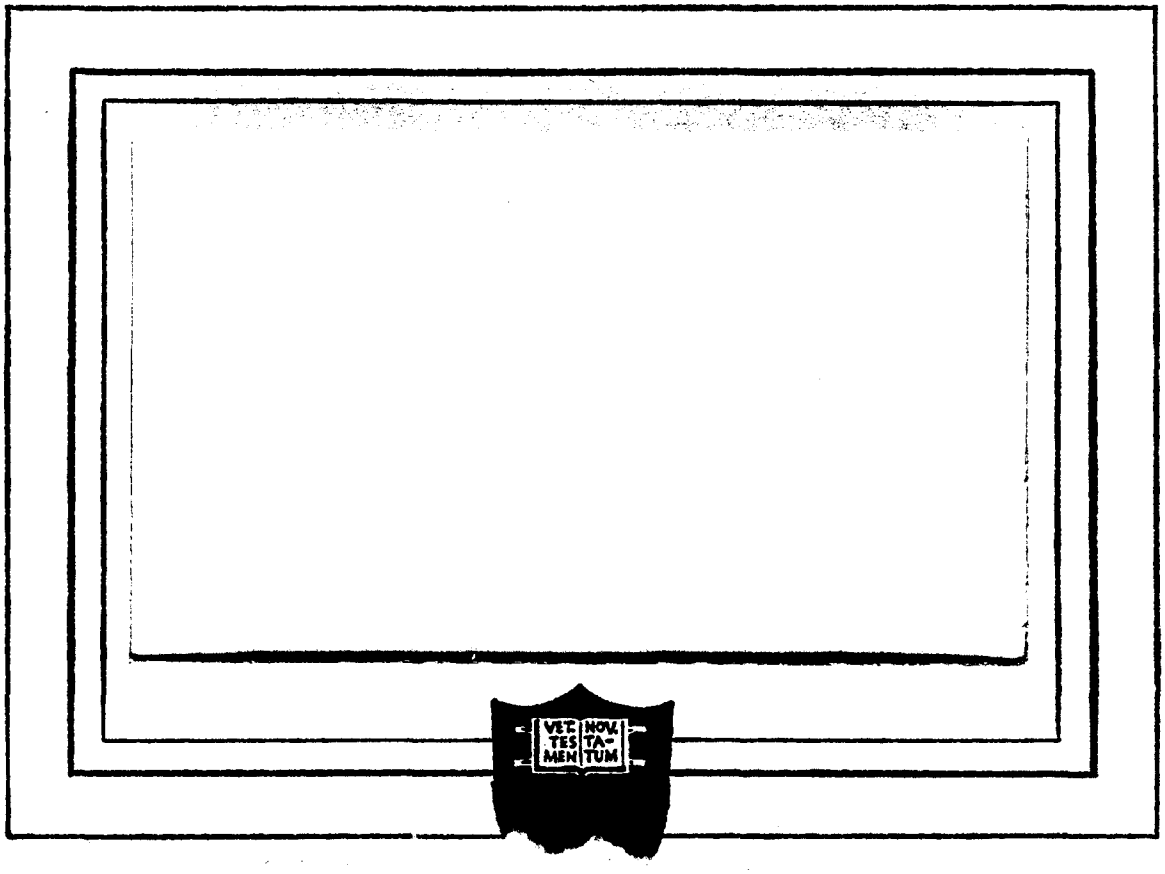

PRINCETON UNIVERSITY

DEPARTMENT OF AEROSPACE AND MECHANICAL SCIENCES

(NASA-CR-69163) PRE-IGNITION AND IGNITION PROCESSES OF METALS Semiannual Progress Report, 1 May - 31 Oct. 1965 J.G. Hansel, et al (Princeton Univ.) 1 Nov. 1965 87 p

N72-75443

Unclas
00/99 42981

Third Semi-Annual Progress Report
To The
National Aeronautics and Space Administration
On NASA Grant NsG-641
On

PRE-IGNITION AND IGNITION PROCESSES OF METALS

1 May 1965 to 31 October 1965

Report No. 760

Prepared by: James G. Hansel
James G. Hansel
Research Staff Member

Arthur M. Mellor
Arthur M. Mellor
Assistant-in-Research

Approved by: Irvin Glassman
Irvin Glassman
Professor
Principal Investigator

1 November 1965

Department of Aerospace and Mechanical Sciences
Guggehnheim Laboratories for the Aerospace Propulsion Sciences
PRINCETON UNIVERSITY
Princeton, New Jersey

I. INTRODUCTION

This report is the Third Semi-Annual Progress Report to the National Aeronautics and Space Administration by Princeton University on NASA Grant NsG-641, Pre-Ignition and Ignition Processes of Metals, covering the period 1 May to 31 October 1965.

The report is divided into four main divisions which cover respectively the physical model of metal ignition and its application to the practical problems of metal pyrophoricity and efficient metal ignition, results of a literature survey, analytical developments, and experimental results. A general self-consistent model which shows regimes of oxidation, ignition, and combustion is presented in the second section. In the experimental portion of the report, results on the ignition and combustion of tantalum, aluminum, magnesium, and molybdenum are discussed. The final section of the report is devoted to a discussion of future research efforts.

II. THE PHYSICAL MODEL OF METAL IGNITION

Because of the possibility of the formation of solid-phase products of metal-oxidizer pre-ignition reactions on the reacting surface, metal ignition can be much more complicated than the ignition of other fuels such as hydrocarbons. At low temperatures this product film is generally protective in the sense that it inhibits the reaction in time, and thus ignition (immediate temperature runaway on the reacting surface ending in steady-state, self-sustained combustion) is impossible to achieve.

1. General Ignition Considerations

Before discussing a general metal-oxidizer system, a treatment of the simpler system in which no solid-phase product forms on the reacting surface will be given. Consider for example a spherical particle whose central point temperature is 298°K. The particle is placed in an oxidizing gas whose temperature at infinity is 298°K. Isothermal reaction is then allowed to procede on the surface at temperature T_s, but, for the sake of simplicity, any gas-phase products are continuously removed as they appear at temperature T_s and are not allowed to participate in any heat transfer to the environment.

In general, two equations may be written for a system enclosing only the reacting surface at a given instant of time: the first is the chemical heat release rate, and the second is the rate of heat loss from the surface to the environment (which includes the volume interior to the surface), where both equations are functions of the surface temperature.

The chemical energy release rate may be written as

$$\dot{q}_{chem} = \dot{m} Q_{chem} \tag{II-1}$$

$$= K e^{-E/RT_s} \left[\sum_{\substack{\text{reactants,} \\ i}} n_i \Delta H_{i,T_s} - \sum_{\substack{\text{products,} \\ j}} n_j \Delta H_{j,T_s} \right] \tag{II-2}$$

where

$$\Delta H_{\ell,T_s} = \Delta H_{f,\ell}^{298} + (H_{T_s} - H_{298})_\ell \qquad (\ell = i, j) \tag{II-3}$$

and where

$\dot{q}_{chem}$ = chemical energy release rate, cal/cm^{2}sec;

$\dot{m}$ = molar reaction rate, mole fuel/cm^{2}sec;

Q_{chem} = chemical energy release, cal/mole fuel;

K = pre-exponential factor, mole fuel/cm^{2}sec;

E = activation energy, cal/mole;

R = univeral gas constant, cal/mole ^oK;

T_s = surface temperature, ^oK;

n_k = number of moles of species K per mole of fuel, mole K/mole fuel;

$\Delta H_{f,K}^{298}$ = standard heat of formation of species K at 298^oK, cal/mole K;

$H_{T,K}$ = enthalpy of species K at T^oK, cal/mole K.

A graph of the form of $\dot{q}_{chem}$ versus T_s is shown in Fig. 1a; the discontinuous rise in $\dot{q}_{chem}$ at constant T_s which is shown would occur at the melting or boiling point of a reactant (i.e., ΔH_f^{298} of the reactant in Eqns. (II-2) and (II-3) would rise discontinuously). By similar reasoning, in the case of metal combustion for which the flame temperature is limited to the boiling point of the oxide, a discontinuous drop in $\dot{q}_{chem}$ would be found at the boiling point of the oxide; this point will not be considered further here. The gradual change to negative slope is due to dissociation of the products which is reflected in largervalues of $\Delta H_{j,T_s}$.

The second equation to be considered is the rate of heat loss at some instant of time from the thin volume surrounding

the surface:

$$\dot{q}_{loss} = K_f \left.\frac{\partial T}{\partial r}\right|_{r=r_{o^-}} + K_g \left.\frac{\partial T}{\partial r}\right|_{r=r_{o^+}} + \epsilon\sigma(T_s^4 - T_r^4) \qquad \text{(II-4)}$$

where

$\dot{q}_{loss}$ = rate of heat loss, cal/cm^{2}sec;

K = thermal conductivity of fuel (subscript f) or oxidizer gas (g), cal/cm sec ^{o}K;

$\left.\frac{\partial T}{\partial r}\right|_{r=r_o}$ = temperature gradient evaluated at the surface ($r=r_o$), either into the fuel (r_{o^-}) or into the oxidizer (r_{o^+}), ^{o}K/cm;

ϵ = surface emissivity, dimensionless;

σ = Stephan-Boltzmann constant, cal/cm^{2}sec (^{o}K)^4;

T_r = effective radiation temperature of the evironment, ^{o}K;

The general form of Eqn. (II-4) is shown in Fig. 1b.

Combining Figs. 1a and 1b (Fig 1c), there will be in general three intersections which define equilibrium conditions for the surface. That which occurs at the lowest temperature is a stable equilibrium (with respect to small perturbations in surface temperature) since

$$\left(\frac{\partial \dot{q}_{chem}}{\partial T_s}\right)\Bigg|_{T_s = T_{oxid}} < \left(\frac{\partial \dot{q}_{loss}}{\partial T_s}\right)\Bigg|_{T_s = T_{oxid}} \qquad \text{(II-5)}$$

The temperature at which this intersection occurs is referred to as the oxidation temperature (T_{oxid}); the intersection has physical significancein that it represents ordinary low-temperature oxidation. Since the slopes of the $\dot{q}_{chem}$ and $\dot{q}_{loss}$ may be nearly tangent at T_{oxid}, this single temperature may be more realistically represented by a temperature range.

The center intersection of the $\dot{q}_{chem}$ and $\dot{q}_{loss}$ curves is said to occur at the critical temperature (T_{crit}). Note that this equilibrium is unstable, since

$$\left(\frac{\partial \dot{q}_{chem}}{\partial T_s}\right)\Bigg|_{T_s=T_{crit}} > \left(\frac{\partial \dot{q}_{loss}}{\partial T_s}\right)\Bigg|_{T_s=T_{crit}} \qquad \text{(II-6)}$$

Furthermore, note that T_{crit} is the classical ignition temperature; it is the spontaneous ignition temperature, that is, it is the lowest initial temperature from which the surface may self-heat to a combustion configuration. However, to avoid confusion with the experimental ignition temperature which will be defined later, this temperature will always be referred to as the critical temperature.

The final intersection occurs at the flame temperature (T_f) and represents a stable equilibrium. Physically, of course, this intersection is the steady-state, self-sustained combustion configuration. Note that, if the radiation term in Eqn. (II-4) is neglected, the intersection occurs at the adiabatic flame temperature. Since in this case the conductive losses in Eqn. (II-4) are equal to the product of the reaction rate and the sensible enthalpy of the reactants, the equations become

$$\dot{q}_{chem} = \dot{q}_{loss} \qquad \text{(II-7)}$$

$$Ke^{-E/RT_s}\left(\sum_{\substack{\text{reactants}\\ i}} n_i \Delta H_{f,i}^{298} - \sum_{\substack{\text{products,}\\ j}} n_j \Delta H_{j,T_s}\right)$$

$$= -Ke^{-E/RT_s} \sum_{\substack{\text{reactants,}\\ i}} n_i (H_{T_s} - H_{298})_i + K_f \frac{\partial T}{\partial r}\Bigg|_{r=r_{o-}}$$

$$+ K_g \frac{\partial T}{\partial r}\Bigg|_{r=r_{o+}} = 0 \qquad \text{(II-8)}$$

$$\therefore \sum_{\substack{\text{reactants,}\\ i}} n_i \Delta H_{f,i}^{298} - \sum_{\substack{\text{products,}\\ j}} n_j \Delta H_{j,T_s} = 0 \qquad \text{(II-9)}$$

which is of course the defining equation for the adiabatic flame temperature.

In defining an ignition temperature it is convenient to choose a definition which is directly related to that of the experimental ignition temperature, usually taken to be the point of most rapid rate of change with time of sample temperature or of light intensity emitted by the sample. Since

$$\frac{mc_p}{S}\frac{\partial T_s}{\partial t} \cong \dot{q}_{chem} - \dot{q}_{loss}$$

where

m = mass of fuel sample, g;

c_p = fuel specific heat, cal/g$^{\circ}$K;

S = sample surface area, cm^2;

t = time, sec,

an appropriate definition of ignition in terms of the $\dot{q}_{chem}$ and $\dot{q}_{loss}$ curves is that temperature at which the magnitude of ($\dot{q}_{chem}$-$\dot{q}_{loss}$) is greatest.

Physically, the ignition temperature (T_{ign}) is the temperature at which immediate inflammation occurs, whereas the critical temperature is the spontaneous ignition temperature; thus an important distinction between these temperatures is

the possibility of an ignition delay time.

It is obviously the ignition rather than critical temperature which is of interest in rocket propulsion applications since a long self-heating period upon attainment of the critical temperature before ignition could be extremely detrimental to ignition efficiency.

The critical and ignition temperatures are demonstrated graphically in Fig. 2a. Only the central portion of the $\dot{q}_{chem}$ and $\dot{q}_{loss}$ curves are reproduced in Fig. 2. Note that as the slope of the $\dot{q}_{chem}$ curve becomes steep in the neighborhood of T_{crit}, T_{ign} and T_{crit} merge and may become indistinguishable.

2. Metal Ignition

It has already been noted that it is the presence of solid-phase products, which form on the reacting surface during the pre-ignition reactions, that complicates metal ignition. In general, the presence of this product film leads to, at low temperatures, a so-called protective oxidation rate (i.e., logarithmic, parabolic, or cubic rate law; see, for example, Kubaschewski, O., and Hopkins, B. E., Oxidation of Metals and Alloys, Second Edition, Butterworths, London, 1962). Protective used in this sense refers to the case in which the rate of chemical reaction decreases with time due to the inhibiting effect of the oxide film. At higher temperatures the rate is generally linear, i.e., non-protective. The transition temperature (T_{trans}) is defined as the lowest temperature at which the transition from a protective to non-protective oxidation rate occurs at the start[1] of the oxidation experiment and is estimated from the empirical oxidation literature for the appropriate metal-oxidizer system.

Note that the linear oxidation rate may be attributed to physical mechanisms other than a porous, non-protective reaction product. For example, if there is a protective, non-porous barrier layer between an outer porous layer and the metal substrate, and if this barrier layer maintains a constant thickness with respect to time, then a linear oxidation rate will be observed for this system. Thus some caution must be exercised in estimating the transition temperature.

The transition from a protective rate law to the linear rate law may be attributed to one of six different physical

[1] There is generally a brief induction period at the start of an oxidation experiment before steady-state conditions are established.

mechanisms:

[a] The volume of oxide formed may be less than the volume of metal used in its formation (i.e., the Pilling and Bedworth ratio (the volume ratio) may be less than one);

[b] The oxide may melt or sublime thus exposing fresh metal surface;

[c] Mechanical stress cracking may result from expansion or contraction due to a phase change or crystallization in scale or substrate;

[d] Mechanical stress cracking may result from a chemical composition change in the film;

[e] Thermal stress cracking may result from large differences in coefficients of thermal expansion of metal and product film;

[f] Mechanical stress cracking may result from a Pilling and Bedworth ratio much greater than one (the volume of oxide formed being much larger than the volume of metal required to form it), perhaps when some critical oxide thickness is attained.

The effect of the transition temperature will be felt in the $\dot{m}$ term of Eqn. (II-1), i.e., in the pre-exponential factor and activation energy of Eqn. (II-2). The presence of the protective product film will lower the reaction rate from the value expected for a clean surface; therefore $\dot{q}_{chem}$ will decrease in the real case. When the transition temperature is attained, the chemical heat release term will approach its value for a clean surface.

The ignition criterion for the two possible cases, $T_{trans} < T_{crit}$ and $T_{trans} > T_{crit}$, is indicated in Fig. 2b and 2c according to the definitions given above. The dashed $\dot{q}_{chem}$ curves indicate the rate for a clean surface. The ignition criterion may be summarized mathematically:

$$\text{if } T_{trans} < T_{crit}, \text{ then } T_{ign} \geqslant T_{crit} \qquad \text{(II-11)}$$

$$\text{if } T_{trans} > T_{crit}, \text{ then } T_{ign} \geqslant T_{trans} \qquad \text{(II-12)}$$

The equal sign will apply in Eqns. (II-11) and (II-12) only if the magnitude of ($\dot{q}_{chem} - \dot{q}_{loss}$) is large at the critical and transition temperatures, respectively (for example, if the $\dot{q}_{chem}$ curve were steep in the neighborhood of the appropriate temperature).

3. Metal Prophoricity

In approaching the problem of metal pyrophoricity, the influence of sample volume on the transition, critical, and ignition temperatures must be examined. It is postulated that the transition temperature will remain constant as the volume of the sample is changed. However, the critical temperature will not remain constant.

Inspection of Eqns. (II-1) through (II-4) reveals only two possible functions of sample volume, the two conduction heat loss terms in Eqn. (II-4). Because $K_g << K_m$,[2] only conduction into the interior of the particle will be considered here.

The dependence of this conduction loss term on sample volume may be evaluated by consideration of a simpler, but related problem. Consider a sphere of radius r_o initially at temperature T=0 except at $r=r_o$ where the temperature is T_s, which is constant in time. The solution of the non-steady Fourier heat conduction equation for this system is[3]

$$T = T_s + \frac{2r_o T_s}{\pi r} \sum_{n=1}^{\infty} \frac{(-1)^n}{n} \sin\left(\frac{n\pi r}{r_o}\right) \exp\{-\alpha n^2 \pi^2 t / r_o^2\} \qquad \text{(II-13)}$$

where all symbols have their previous meanings and where

n = summation variable taking all integral values between 1 and ∞, dimensionless;

α = fuel thermal diffusivity, cm^2/sec.

---

[2] McAdams, W.H., Heat Transmission, Third Edition, McGraw-Hill, New York, 1954.

[3] Carslaw, H.S., and Jaeger, J.C., Conduction of Heat in Solids, Second Edition, p. 233, Oxford University Press, London, 1959.

Since the series (II-13) is uniformly convergent for $t > o$ and $o \leq r \leq r_o$,[4] we may differentiate term by term and multiply by the thermal conductivity of the fuel (K_f) to obtain the conduction heat loss term:

$$\dot{q}_{cond}(r,t) = K_f \frac{\partial T}{\partial r} \tag{II-14}$$

$$= \frac{2 r_o K_f T_s}{\pi r} \sum_{n=1}^{\infty} \frac{(-1)^n}{n} \left[\frac{n\pi}{r_o} \cos\left(\frac{n\pi r}{r_o}\right) - \frac{1}{r} \sin\left(\frac{n\pi r}{r_o}\right) \right] \exp\left\{-\alpha n^2 \pi^2 t / r_o^2\right\} \tag{II-15}$$

Evaluating $\dot{q}_{cond}$ at the surface:

$$\dot{q}_{cond}(r_{o-}, t) \equiv \dot{q}_{cond,s} \tag{II-16}$$

$$= \frac{2 K_f T_s}{r_o} \sum_{n=1}^{\infty} \exp\left\{-\alpha n^2 \pi^2 t / r_o^2\right\} \tag{II-17}$$

in the limit as $r \rightarrow r_o$.

If then

$$\frac{\partial \dot{q}_{cond,s}}{\partial r_o} > 0 \tag{II-18}$$

---

[4] Carslaw, H.S., and Jaeger, J. C., Conduction of Heat in Solids, Second Edition, pp 94-95, Oxford University Press, London, 1959.

it is apparent that a small decrease in r_o (or the sample volume) will decrease the conduction heat loss rate accordingly. Thus the critical intersection of the $\dot{q}_{chem}$ and $\dot{q}_{loss}$ curves will move toward lower temperatures as the volume of the sample is decreased, and

$$\frac{\partial T_{crit}}{\partial r_o} > 0 \qquad \text{(II-19)}$$

i.e., the critical temperature of the system will decrease as the radius (or volume) of the sample is decreased.

From Eqn. (II-17)

$$\frac{\partial \dot{q}_{cond,s}}{\partial r_o} = 2K_f T_s \sum_{n=1}^{\infty} \exp\{-\alpha n^2 \pi^2 t / r_o^2\} \left[-\frac{1}{r_o^2} + \frac{2\alpha n^2 \pi^2 t}{r_o^4} \right] \qquad \text{(II-20)}$$

Since the term outside the brackets on the right hand side of Eqn. (II-20) is positive, the criterion for Eqns. (II-18) and (II-19) becomes

$$\sum_{n=1}^{\infty} \frac{2\alpha n^2 \pi^2 t}{r_o^2} > 1 \qquad \text{(II-21)}$$

or

$$\frac{2\alpha \pi^2 t}{r_o^2} > \frac{1}{\sum_{n=1}^{\infty} n^2} = 0 \qquad \text{(II-22)}$$

Since the property of uniform convergence applies only for $t > o$, the criterion (II-19) is satisfied for all finite values of r_o.

The same conclusion can be reached on purely physical grounds. Taking as the appropriate size index the surface area-volume ratio (S/V) which indicates the approximate magnitudes of the total chemical heat release and total heat capacity of the system, the effect of heat loss will increase with decreasing S/V (larger systems). Thus the critical temperature will increase with increasing particle size. Note that the transition temperature still must be exceeded before ignition can occur and that as the sample size is decreased ignition may shift from that depicted in Fig 2b ($T_{crit} > T_{trans}$) to that in Fig. 2c ($T_{crit} < T_{trans}$).

After the volume of the sample exceeds a certain value, as far as events on the surface are concerned the volume is essentially infinite. At and above this critical size the critical temperature becomes relatively independent of size; such samples are said to be in the bulk configuration.

Results of the literature survey on the size effect in metal ignition will be given in Section III of this report.

In summary, it has been shown that the critical temperature of a given metal-oxidizer system decreases with decreasing system size. In other words, a small particle may self-heat to the transition temperature and thus ignition, whereas a larger sample will not. Note that no assumption has been made concerning the initial condition of the metal particle when it is exposed to the oxidizer, i.e., it is not necessary that the surface be free of oxide initially. As long as $\dot{m}$ in Eqn. (II-1) is non-zero, the possibility of eventual ignition exists. ($\dot{m}$ is zero only if the asymptotic oxide thickness for the appropriate initial temperature is present on the particle initially.)

4. Increased Ignition Efficiency

Since the critical temperature of a given metal-oxidzer system decreases as the metal sample volume is decreased, the transition temperature will eventually become the controlling factor in metal ignition. For some metals (e.g.,

Mg and Ca[5]) which have low transition temperatures in oxygen inefficient ignition would not be expected, but with other metals such as Al and Be[5] with high transition temperatures, difficulties have been encountered in metal combustion applications such as chemical rocket systems.

Lowering the transition temperature is equivalent to destroying the protective quality of the product film at a low temperature or eliminating its formation entirely. An excellent example of the former technique is the amalgamation of aluminum, and this metal so treated exhibits lower ignition temperatures than that with the ordinary thermal oxide film (336,332)[6].

The latter technique is examplified by coating clean Al with Mg or Ca. Assuming that alloying does not occur, it would be hoped that the coating metal would react preferentially during the pre-ignition time, and that its ignition would be controlled by its low transition temperature. After the coating metal had ignited, the clean Al (or Be) substrate would ignite and burn during the subsequent temperature rise without the limitations imposed by its high transition temperature.

Calculations of the necessary coating thickness are currently in progress and will be described in detail in Section IV of this report.

The next section is devoted to a brief review of the results of the literature survey.

---

[5]Numerical values of transition temperature will be estimated in Section III.

[6]Numbers in parantheses refer to references listed at the end of this report.

III. THE LITERATURE SURVEY

A thorough literature survey, covering references dating from about 1910 to the present, on the oxidation and ignition of certain metals is in progress. At this time about 475 references have been surveyed; about 300 references remain. The metals of study are aluminum, magnesium, titanium, zirconium, tantalum, molybdenum, calcium, silicon, uranium, beryllium, and lithium. Experimental investigations of the ignition and combustion of several of these metals have been completed (Al, Mg, Ta) or are in progress (Ca, Mo) in this laboratory. The particular oxidizing atmospheres of interest are oxygen, nitrogen, carbon dioxide, and water vapor.

Examination of the oxidation literature has led to estimates of transition temperatures for several metal-oxidizer systems; the system, transition temperature, and transition mechanism are listed in Table 1. All temperatures except that for $Zr-O_2$ may be taken accurate to $\pm$ 50°C. Detailed discussions of these estimates may be found in previous progress reports.[7]

Estimates of critical temperature for bulk samples are available only for Al and Mg: that of the $Al-O_2$ system is $\sim$ 1000° C[7] and that of the $Mg-O_2$ or Mg-air system is $\sim$ 585°C. In Fig. 3 the initial temperature vs. ignition delay time is shown for the latter two systems. The asymptotic critical temperature is seen to be on the order of 585°C. Ignition was defined as the instant before a flame appeared in these experiments.

All ignition temperatures obtained from the literature survey (i.e., Refs. (1) through (483)) are shown in Tables 2-12 and Figs. 4-8, correlated with respect to size, condition, and oxidizing atmosphere. For the purposes of these charts, pressure effects, surface treatment prior to experimentation, and so forth have been disregarded. The nomenclature used in the tables and graphs is as follows: DD indicates a dust dispersed in the gas of interest; QP indicates a quiescent pile of powder; B indicates a large bulk sample; and SP indicates a single particle dropped through the oxidizing gas. The appropriate references are listed at the end of the report.

Although it is not expected a priori that correlations exist between the various sample configurations, it is hoped that data for each would be self-consistent.

Some sizes in the tables, and all sizes in the figures are expressed in terms of the surface area to volume ratio with units

---

[7] See also: Mellor, A. M., and Glassman, I. "A physical criterion for metal ignition," to be published in Phyrodynamics.

of reciprocal millimeters.

Considering first the bulk ignition, in general the agreement is excellent between the experimental results and the predictions based on the ignition criterion. In particular, knowledge of the critical temperatures for bulk Mg and Al in oxygen allows classification of their ignition mechanisms as that shown in Figs. 2b and 2c respectively.

However, the size effect in ignition is not as clear. Through the ignition criterion, recall that the critical temperature changes with sample size. Becuase of the nature of the DD, QP, and SP experiments, the temperature reported is the critical rather than ignition temperature as defined here. That is, the initial temperature of the furnace used in these experiments is taken as the ignition temperature. Unfortunately, no ignition delay times are reported.

Turning to Tables 2-12, although the reported temperatures are generally lower than those for the bulk configurations, the data are quite inconsistent, and no significant trends with respect to size are observed except in isolated cases. The nature of these results is most likely due to the fact that a great deal of data is presented in terms of sieve sizes, which of course yield no information of a size distribution and thus of some average size.

For a few metals in certain oxidizers enough references giving specific size information have been found to warrant graphing the ignition temperature vs. the surface-volume ratio, These graphs are shown in Figs. 4-8.

With the exception of Mg (Figs. 4 and 5), the expected trend is observed: T_{ign} decreases with decreasing sample size (increasing S/V). Recall that, through the ignition criterion, the variation in T_{crit} is actually observed since T_{trans} is independent of size. Since any ignition delay time is usually not reported for this type of data, it is impossible to distinguish between T_{crit} and T_{ign}.

Some of the agreement shown in Figs. 7 and 8 is undoubtedly fortuitous, since most of it was taken from various papers by Schnizlein and co-workers ((30), (231), (306)).

In summary, this brief discussion on the available literature on metal ignition demonstrates that the model and criterion of ignition proposed in Section II of this report is adequate to explain earlier experimental work. However, much further critical experimentation is necessary to examine the model in

more detail. For example, the size effect must be more clearly understood before predictions can be made for the ignition of micron size particles currently in use in rocketry; the literature is most inconclusive on this point. Also, experimental determinations of T_{crit} as a function of size must be made.

A 10 kw induction furnace and its associated apparatus is being made available to the program and is expected to be operational in February 1966. The largest metal samples to be used are cylinders of approximately 2" length and 1" diameter. The independent variables in the furnace experiments will be the metal, gas composition and total pressure (which will vary over the same ranges used in the present wire experiments), and metal sample size (S/V) . The major proposed experiments to be performed over the range of independent variables are the following:

(1) The ignition temperature experiment in which the sample is heated to ignition (i.e., to appearance of a flame) in the specified oxidizer. The ignition temperature is the sample temperature the instant before the flame appears.

(2) The critical temperature (isothermal furnace) experiment in which the sample is heated to a specified temperature in an inert gas or an oxidizer. If, as the furnace temperature is maintained constant, the sample self-heats to ignition, then the furnace temperature is at or above the critical temperature.

(3) The adiabatic sample experiment in which the environment and sample temperatures are kept equal. In an oxidizing atmosphere the sample should always ignite eventually.

Of these experiments, the third is considered to be the most difficult to realize experimentally; the first two experiments will be begun upon arrival of the apparatus.

In the next section of the report the analytical developments made during the report period will be discussed.

IV. ANALYTICAL DEVELOPMENTS

Because of certain errors made in the analysis presented in the Second Semi-Annual Progress Report, a revised analysis will be outlined here.

Under consideration is the general problem of a spherical particle in an oxidizing atmosphere. The particle consists of an inner metal sphere surrounded by an oxide shell. The radius of the inner metal sphere r_s is a function of time since the metal is allowed to oxidize. Initially the metal radius is r_o and the temperature of the metal-oxide interface is T_o.

The following assumptions are made:

(1) All heat addition (i.e., the chemical reaction) occurs at the metal-oxide interface. Thus the diffusion of oxidizer through the oxide scale is required for reaction. This assumption is valid in the case of many metal-oxidizer systems.

(2) During the oxidation process, the surface of the metal is smooth, and the metallic portion of the particle retains spherical symmetry. Thus the metal temperature is a function only of radius.

(3) All thermal properties of the metal are independent of temperature.

In the first solution of the problem, known as the adiabatic metal problem, the following assumption is added:

(4) The oxide film is a perfect thermal insulator, and thus all heat release occurring at the metal-oxide interface is conducted into the interior of the metal sphere. The strength of this assumption in the real physical situation is examined by comparison of the thermal conductivities of metal and oxide; for Al and Mg the ratios of the metal thermal conductivity to that of the oxide are 6.13 and 4.19 respectively.[8]

Note that because a thin control volume surrounding the metal-oxide interface at which reaction is occurring is not adiabatic due to the conduction loss into the interior of the metal, the critical temperature is not eliminated from the problem. However, the adiabatic metal problem does allow investigation of the importance of the interior of the metallic portion

---

[8] Handbook of Chemistry and Physics, 44th Edition, Chemical Rubber Publishing Company, Cleveland, 1961.

of the particle as a heat sink.

Under the above conditions the problem can be formulated mathematically as follows: the Fourier equation for the temperature distribution must be solved:

$$\frac{\partial T}{\partial t} = \alpha\left(\frac{\partial^2 T}{\partial r^2} + \frac{2}{r}\frac{\partial T}{\partial r}\right) \qquad \text{(IV-1)}$$

subject to the initial condition

$$T(t=0) = T_o \quad \text{at} \quad r = r_s = r_o \qquad \text{(IV-2)}$$

and the boundary conditions

$$T \quad \text{finite at } r=0 \text{ for finite } t \qquad \text{(IV-3)}$$

$$\left.\frac{\partial T}{\partial r}\right|_{r=r_{s-}} = \frac{\dot{m}}{K} Q \qquad \text{(IV-4)}$$

where all symbols have their previous meanings and subscript s- indicates conditions in the metal adjacent to the metal-oxide interface (in the following this will be denoted by subscript s), and Q is the heat of reaction in cal/g metal. Note that since the heat release occurs only at the metal-oxide interface it may be included only in the boundary condition (IV-4), and that the solution is physically meaningful only for $r \leq r_s$.

If T and r are non-dimensionalized with their initial values:

$$\theta \equiv T/T_o \qquad \text{(IV-5)}$$

$$\xi \equiv r/r_o \qquad \text{(IV-6)}$$

the statement of the problem becomes:

$$\frac{r_o^2}{\alpha}\frac{\partial\theta}{\partial t} = \frac{\partial^2\theta}{\partial\xi^2} + \frac{2}{\xi}\frac{\partial\theta}{\partial\xi} \qquad \text{(IV-7)}$$

$$\theta(1,0) = 1 \qquad \text{(IV-8)}$$

θ finite at $\xi = 0$ for finite t (IV-9)

$$\left.\frac{\partial\theta}{\partial\xi}\right|_{\xi=\xi_s} = \frac{r_o}{T_o}\frac{\dot{m}}{K}Q \qquad \text{(IV-10)}$$

The problem is solved by the method of separation of variables which yields the general solution:

$$\theta(\xi,t) = \sqrt{\frac{2}{i\pi\beta}}\frac{c}{\xi}\sin i\beta\xi\,\exp\{\alpha\beta^2 t/r_o^2\} \qquad \text{(IV-11)}$$

where c and β are arbitrary constants (β is the separation constant and is restricted to real values), and (IV - 9) has been applied. From Eqn. (IV-8):

$$c = \sqrt{\frac{i\pi\beta}{2}}\frac{1}{\sin i\beta} \qquad \text{(IV-12)}$$

thus

$$\theta = \frac{\sin i\beta\xi}{\xi\sin i\beta}\exp\{\alpha\beta^2 t/r_o^2\} \qquad \text{(IV-13)}$$

$$\theta = \frac{\sinh\beta\xi}{\xi\sinh\beta}\exp\{\alpha\beta^2 t/r_o^2\} \qquad \text{(IV-14)}$$

To evaluate β the other boundary condition, Eqn. (IV - 10), is used:

$$\left.\frac{\partial\theta}{\partial\xi}\right|_{\xi=\xi_s} = \frac{r_o\dot{m}Q}{KT_o} \qquad \text{(IV-15)}$$

$$\left.\frac{\partial\theta}{\partial\xi}\right|_{\xi=\xi_s} = \frac{\exp\{\alpha\beta^2 t/r_o^2\}}{\sinh\beta}\left[\frac{\beta\cosh\beta\xi_s}{\xi_s} - \frac{\sinh\beta\xi_s}{\xi_s^2}\right] \qquad \text{(IV-16)}$$

Since the primary area of interest in the solution is below the transition temperature, only parabolic oxidation rate laws will be considered here. These are usually expressed as

$$(\Delta m)^2 = K_p t \qquad \text{(IV-17)}$$

where

Δm = change in mass of pure metal per unit area, g metal/cm^2;

K_p = parabolic rate constant, (g metal)^2/cm^4sec.

Recall that $\dot{m}$ in Eqn. (IV-15) is expressed in g metal/cm^2sec. Thus

$$\dot{m} = \frac{d}{dt}(\Delta m) = \frac{K_p}{2\Delta m} \qquad \text{(IV-18)}$$

Now

$$\Delta m(t) = \rho\,\Delta V(t)/A(t) \qquad \text{(IV-19)}$$

$$= \frac{4}{3}\pi\rho(r_o^3 - r_s^3)/4\pi r_s^2 \qquad \text{(IV-20)}$$

$$= \frac{\rho}{3} r_o\left(\frac{1}{\xi_s^2} - \xi_s\right) \qquad \text{(IV-21)}$$

Also

$$t(\xi_s) = \frac{(\Delta m)^2}{K_p} = \frac{\rho^2 r_o^2\left(\frac{1}{\xi_s^2} - \xi_s\right)^2}{9K_p} \qquad \text{(IV-22)}$$

Substituting Eqs. (IV -18), (IV-21), and (IV-22) into Eqn. (IV-16):

$$\frac{3K_pQ}{2\rho KT_o\left(\frac{1}{\xi_s^2}-\xi_s\right)} = \frac{\exp\left\{\alpha\beta^2\rho^2\left(\frac{1}{\xi_s^2}-\xi_s\right)^2/9K_p\right\}}{\sinh\beta}\left[\frac{\beta}{\xi_s}\cosh\beta\xi_s - \frac{1}{\xi_s^2}\sinh\beta\xi_s\right] \qquad \text{(IV-23)}$$

Since β is constant, it may be evaluated from Eqn. (IV-23) for any ξ_s. Choose $\xi_s = \frac{1}{2}$:

$$\frac{3K_pQ}{7\rho KT_o} = \frac{\exp\{12.25\alpha\beta^2\rho^2/9K_p\}}{\sinh\beta}\left[2\beta\cosh\beta/2 - 4\sinh\beta/2\right] \qquad \text{(IV-24)}$$

Define

$$A \equiv \alpha\rho^2/K_p \qquad \text{(IV-25)}$$

$$B \equiv K_pQ/\rho KT_o \qquad \text{(IV-26)}$$

$$\therefore \frac{3}{14}B = \frac{\exp\{12.25A\beta^2/9\}}{\sinh\beta}\left[\beta\cosh\beta/2 - 2\sinh\beta/2\right] \qquad \text{(IV-27)}$$

β is evaluated on a computer from Eqn. (IV-27) using the Newton-Raphson technique.

Note that A and B are the dimensionless parameters which completely characterize the metal-oxidizer system under study.

Selection of the parameters α, ρ, K_p, Q, and K is currently in progress. T_o will be varied from 100^oK to that integral multiple of 100^oK just below the transition temperature, in steps of 100^oK. The solution will be terminated when the metal-oxide interface temperature exceeds the transition temperature, since in metal pyrophoricity this temperature controls ignition. Although it is assumed that ignition will occur if only the interface reaches the transition temperature, which is inconsistent with the physical model which requires that the entire oxide reach the transition temperature, the effect of only the interior of the metal as a heat sink is investigated.

Note that the distance which the metal-oxide interface has receded from its initial position when its temperature equals the transition temperature is the unknown coating metal thickness required in the binary ignition model (see Section II-4). In this case the metal sphere is considered to be composed of two immiscible metals, one applied as a thin coating on the other. It is assumed that the thermal properties (α, ρ, and K) of the binary system are given by the inner metal, which is present in excess, and that the chemical properties (K_p, Q, and T_{trans}) are given by the coating metal.

Results of both the single and binary adiabatic metal problems described above will become available during the next report period.

It is of interest to eliminate assumption (4) from the problem to determine its influence on the solution. For this purpose a conduction heat loss into the oxide shell is allowed; assumption (4) is deleted from the problem and the following two assumptions are added:

(5) The temperature profile through the oxide film is linear and the outer surface remains at T_o. Because the temperatures involved are relatively low, radiation will again be neglected. This assumption is not particularly good since the low thermal conductivity of the oxide tends to prevent the establishment of a linear temperature profile. Nevertheless, solution of the problem under this assumption should lend some insight into the effect of a heat loss from the metal-oxide interface to the ambient environment.

(6) The oxide shell formed is coherent, continuous, and has spherical symmetry; thus the distance the interface has receded can be related to the oxide thickness at any time through the Pilling and Bedworth ratio.

The boundary condition (IV-4) then becomes:

$$K_m \left.\frac{\partial T}{\partial r}\right|_{r=r_{s-}} = \dot{m}Q - K_{ox} \left.\frac{\partial T}{\partial r}\right|_{r=r_{s+}} \qquad \text{(IV-28)}$$

where all symbols have their previous meanings, K is the thermal conductivity of metal (subscript m) or oxide (subscript ox), and ($K_{ox}\partial T/\partial r|_{r=r_{s+}}$) is the conduction heat loss through the oxide.

Under assumption (5), Eqn. (IV-28) becomes:

$$K_m \left.\frac{\partial T}{\partial r}\right|_{r=r_{s-}} = \dot{m}Q - K_{ox} \frac{T_s - T_o}{r_{ox} - r_s} \qquad \text{(IV-29)}$$

where r_{ox} is the total particle radius at any time. Non-dimensionalizing as before:

$$\left.\frac{\partial \theta}{\partial \xi}\right|_{\xi=\xi_{s-}} = \frac{r_o \dot{m} Q}{K_m T_o} - \frac{K_{ox}}{K_m} \frac{\theta_s - 1}{\xi_{ox} - \xi_s} \qquad \text{(IV-30)}$$

Through assumption (6) and the definition of the Pilling and Bedworth ratio (V_{ox}/V_m):

$$\frac{V_{ox}}{V_m} \equiv \gamma = \frac{4/3\,\pi(r_{ox}^3 - r_s^3)}{4/3\,\pi(r_o^3 - r_s^3)} \qquad \text{(IV-31)}$$

$$= \frac{\xi_{ox}^3 - \xi_s^3}{1 - \xi_s^3} \qquad \text{(IV-32)}$$

$$\therefore \xi_{ox} = \sqrt[3]{\xi_s^3 + \gamma(1 - \xi_s^3)} \qquad \text{(IV-33)}$$

where γ is taken from the oxidation literature for the particular metal-oxide system.

Combination of Eqns. (IV-16), (IV-30), and (IV-33) will yield an equation in β and the variables ξ_s, $\theta_s(\xi_s)$, $t(\xi_s)$, and $\dot{m}(\xi_s)$. The latter two variables may be eliminated through Eqns. (IV-18), (IV-21), and (IV-22), leaving an equation for β in terms of ξ_s and θ_s. A first approximation for $\theta_s(\xi_s)$ can be obtained from the adiabatic metal problem and an iteration for β can be established. Work will procede on this problem as time permits.

The next section of the report is devoted to a discussion of the results of experimental investigations of the ignition and combustion of tantalum, aluminum, magnesium, and molybdenum. Tantalum was selected for ignition studies because of its high Pilling and Bedworth ratio, aluminum and magnesium becuase of their well-known transition, critical, and ignition temperatures, and molybdenum because of its extremely volatile oxide.

V. EXPERIMENTAL RESULTS

This section of the report is a discussion of the experimental results obtained in the so-called wire-burning apparatus during the report period. The general characteristics of the apparatus are described in detail elsewhere.[7,9]

1. The Ignition and Combustion of Tantalum

Metallurgical grade tantalum (99.92% Ta, major impurities Cb (.030%) and O_2 (.010%)) was obtained in wire form (.030" diameter) from the Kawecki Chemical Company. All samples were 11 cm in length and were mounted in the electrodes in an "L" configuration. The electrical voltage rate rise used to heat the samples was about .125 v/sec.

In Fig. 9 is shown the montage for the various reaction regimes of Ta wires, including typical photographs for the reaction mechanisms and products. The four reaction regimes are shown as a function of gas composition and pressure; the data points were taken at total pressures of 50,100,300,500 torr (1 torr=1 mm Hg), and 1, 2, and 5 atm in pure O_2, CO_2, and Ar and 50-50 mixtures of these gases. Water vapor experiments were also conducted in 50-50 mixtures of H_2O-O_2, H_2O-Ar, and H_2O-CO_2 at total pressures of 50, 100, and 200 torr.

The reaction mechanisms and products are described in detail in the Second Semi-Annual Progress Report, and will be repeated verbatim here so that the data obtained during the present report period will be more meaningful.

Regime one occurred in pure O_2 at all pressures investigated and in O_2-Ar and O_2-CO_2 at 5 atm. It is characterized by a white, apparently solid-phase combustion process. Data on the boiling points of Ta and Ta_2O_5 are not available, and thus the vapor-phase combustion criterion, that the boiling point of the oxide be higher than that of the metal, may not be examined.

During the ohmic heating period, the wire slowly and continuously started to glow orange-red. Suddenly near the center of the wire a white-hot solid-phase reaction zone

[9] Brzustowski, T.A., and Glassman, I. pp. 117-158 in Heterogeneous Combustion, Wolfhard, H.G., Glassman, I., and Green, L., Jr., editors, Academic Press, New York, 1964.

appeared and spread toward the electrodes. This event is defined as ignition. Consumption of the wire resulted in its breaking near the center. Combustion continued as molten drops flowed down the wire.

If the combustion zone regressed as far as the electrodes, violent fragmentation occurred when the zone contacted the electrode and was quenched. In pure O_2 at pressures of 300 torr and greater, at the electrode the molten sample expanded, burst, and contracted, then repeating this cycle several times.

The products of combustion, a mixture of α- and β- Ta_2O_5 (see Table 13), were glassy and brown, black and white in color. They usually assumed spherical shapes of several mm diameter and less. Where falling drops had been quenched at the bottom of the chamber, the products were generally flaky.

Regime two consists of the low pressure region in O_2-Ar and most of the pure CO_2, O_2-CO_2, and CO_2-Ar ranges, as is shown in Fig. 9. Strictly speaking, this regime is not characterized by either ignition or combustion: the oxidation reaction which occurs is simply distinguished from the melting which occurs in pure Ar.

The wire attained a dull orange-red glow as it was heated. Then the intensity of the light emitted by the sample began to decrease. The diameter of the sample grew and large macrocracks appeared on its surface, as is shown in Fig. 10 (50% O_2-50% Ar, 100 torr). (Fig. 10 is also shown in the lower right-hand corner of regime two in Fig. 9.) Simultaneously the current passing through the sample began to decrease. Usually the wire did not break, and the current ultimately reached a value less than one ampere.

This mechanism is attributed to ordinary oxidation of the sample. The decrease in current is attributed to the increase in resistance due to consumption of the metal and thus the decrease in conductive area (recall that Ta_2O_5 is an excellent dielectric). As less electrical energy was supplied, and thus the temperature of the sample decreased, its brightness decreased. The surface macrocracks result from the extremely high Pilling and Bedworth ratio of Ta_2O_5, which is equal to 2.50.

The products of oxidation were usually found to be in the original wire shape. The macrocracks were easily visible to the naked eye. In CO_2 and CO_2-Ar atmospheres, and in O_2-Ar atmospheres at pressures of 100 torr and less,

the product was grey-black in color. The products were composed of α- and β- Ta_2O_5; in CO_2 and CO_2-Ar mixtures TaC was also formed. In O_2-Ar at pressures greater than 100 torr, they were brown-white and consisted of both allotropic forms of Ta_2O_5.

In pure CO_2 at total pressures of 300 torr and greater, and in 50% CO_2-50% Ar mixtures where the CO_2 partial pressure was equal to or greater than 250 torr, a localized white glow emanating from the center of the wire cross-section occurred after the rest of the wire had ceased to glow, as is shown in Fig. 11. This small white spot persisted for times on the order of a minute. Occasionally discontinuous jumps in current (i.e., arcing) were observed during this time. A few tiny sparks were seen in the gas surrounding the sample. Most likely this mechanism is a local hot spot at a point where the conducting metallic cross section is small. Recall that in a series circuit the most power is dissapated in the largest resistance.

Regime three was observed in O_2-Ar and O_2-CO_2 mixtures at the higher pressures. The mechanism is simply a combination of those of Regimes one and two, with the oxidation reaction occurring first.

In regime four, at the lower pressures in CO_2 and CO_2-Ar, only certain small sections of the wires oxidized. The experiment terminated when the wire melted and broke. The wire was grey-black in color; its cross-sectional area was large in places where molten beads had solidified when the wire broke and the electrical heating ceased. In both regimes three and four both allotropic forms of the oxide were found (see Table 13).

In pure CO_2 at 50 and 100 torr, tiny bubbles appeared and burst before the wire broke. In mixtures of O_2-Ar, O_2-CO_2, and CO_2-Ar at total pressures between 300 torr and 1 atm (i.e., sections of regimes two and three), larger and more numerous bubbles preceded the oxidation reaction. A few Ta wires which were annealed at nine volts for five minutes in vacuum in the chamber also behaved in this manner. It was felt that this pretreatment before performing the usual experiments should eliminate the appearence of the bubbles if they were due to outgassing, but since they appeared despite the pretreatment, the bubbles are now thought to be small pustules of oxide formed during the ohmic heating.

In pure H_2O and H_2O-Ar mixtures the mechanism of regime two was observed. The cracked products were grey-black, but slightly more white in color than those found previously.

In H_2O-CO_2 mixtures the oxidation reaction again was observed and formed typical grey-black products. At 200 torr (the highest total pressure investigated), the small local white glow, which was previously found for CO_2 partial pressures of 250 torr and greater (in regime two), occurred.

In H_2O-O_2 mixtures, the combustion mechanism of regime one was observed at all pressures investigated (50, 100, and 200 torr). Products similar to those described for regime one were observed.

In Table 14 are shown the averaged values of initial weight, recovered sample weight, total power supplied at ignition, at breaking, and at the maximum current attained (in the oxidation reactions of regimes 2 and 4), total resistance at ignition, at breaking, and at the maximum current attained, and total burning time. These values are classified according to reaction regime and are subdivided with respect to gas composition. The melting values (pure Ar) and those obtained in H_2O mixtures are also included.

The most significant trend observed in the data was that in regime 1 the ignition and breaking values of total power and resistance approached each other; that is, the wire broke more quickly after ignition as the total pressure was increased. Most likely the wire breaks when it attains the metal melting point of 2990°C[10], which is essentially independent of pressure. Thus this trend indicates that either the ignition temperature increases with increasing pressure or that at the higher pressures where the oxidizer diffuses to the wire more rapidly, increased reaction rates bring about a higher rate of temperature rise in the sample. Since ignition depends primarily on low-temperature, solid-state oxidation reactions (through the transition temperature), which most likely would be relatively independent of pressure, the latter explanation of this phenomenon is regarded to be more appropriate.

---

[10]The oxide melting point is 1872°C, and thus Ta_2O_5 most likely is the molten substance observed in the combustion mechanism of regime 1. (Recall that the wire retains its original L-shape even long after its breaking.) Data are taken from Kubaschewski, O., and Hopkins, B.E., Oxidation of Metals and Alloys, Butterworths, London, 1962.

The total burning time in regime 1 was observed to decrease with increasing total pressure. This is also attributed to increased reaction rates at the higher pressures.

The values with asterisks at the bottom of Table 14 are the averages of a few so-called self-sustained experiments which were performed. The purpose of these experiments is to separate true combustion reactions from ordinary oxidation reactions, where combustion is defined as a fast self-sustained chemical reaction occurring in a zone from which light and heat are emitted. On the other hand, oxidation is a slower reaction which under the conditions of this experiment requires electrical heating for its maintenance.

The self-sustained experiments were performed by heating the wire in the usual manner and then suddenly stopping the electrical input at a time in the heating history before the wire would ordinarily break. For example, if the electrical heating were stopped a few tenths of a second after the white solid-phase ignition zone of regime 1 appeared, the ignition flame continued to spread. However, the combustion mechanism of regime 3 occurred rather than that of regime 1. This simply indicates a lower mean temperature along the wire, which is consistent. Thus regime 1 is considered to be combustion as defined above.

If however, the electrical heating was discontinued at or after the current attained its maximum value in regime 2, the wire ceased to glow immediately. Furthermore, as can be seen in Table 14, the weight gain of the sample was less in this case. Examination of the products of reaction showed that a metallic cross section was still visible to the naked eye, whereas it was almost never visible if the experiment was allowed to proceed to completion. Therefore regime 2 is thought to be an ordinary oxidation reaction.

Spectra of the flame of regime 1 were taken at 50 torr of pure O_2, where the longest burning times were observed; only continuum emission, most likely resulting from the molten oxide, was found. This result indicates[11] that no gas phase species are radiating in the visible spectrum between the molten oxide and the spectrograph, but sheds

---

[11] The range of the spectrograph used in these investigations is 3700 to 7400 Å in first order. Both Ta and TaO emit in this spectral region.

no light on the processes occurring inside of the molten oxide; it may be taken as a further substantiation of solid-phase rather than vapor-phase combustion.

In summary, it is noted immediately that if there were no effect of CO_2 on the combustion of tantalum, then the upper two-thirds of Fig. 9 would be symmetric with respect to the pure oxygen line. Since the appearence of regime three (the combination of combustion and oxidation) occurs at higher pressures in O_2-CO_2 than in O_2-Ar, it is concluded that CO_2 impedes the Ta-O_2 reaction. This conclusion has obvious significance in tantalum applications for canning nuclear fuel rods where CO_2 might be used as a coolant.

On the other hand, water vapor has the opposite effect: in 50%H_2O-50%O_2 mixtures at pressures of 200 torr and below the combustion mechanism (regime one) was observed, whereas in both 50%Ar-50%O_2 and 50%CO_2-50%O_2 mixtures in the same pressure range only the oxidation reaction (regime two) occurred.

2. The Ignition and Combustion of Aluminum

To complete the study of the ignition and combustion of unanodized aluminum which has been conducted over the last few years, it was necessary to perform experiments in pure H_2O at 50 and 100 torr, and in 50%-50% mixtures of H_2O-O_2, H_2O-CO_2, and H_2O-Ar at total pressures of 50, 100, and 200 torr.

One would expect that the ignition temperature of aluminum in these gases would be equal to the melting point of Al_2O_3 on the basis of the results reviewed in Section III. However, since the metal melts at 660°C, it is necessary that the molten metal be supported by an oxide coat so that the ohmic heating process continue after the metal has melted. At these low oxidizer pressures one would not necessarily expect that enough oxide would form to serve this purpose.[12] The 5 to 10μ thick anodized layer on the anodized wires used in earlier investigations is sufficient.

The behavior of the sample during the heating period[13] was the same in pure H_2O, pure Ar, in the H_2O-Ar and

---

[12] Early results with anodized aluminum wires in O_2-Ar indicated that at least 200 torr of O_2 were required in the ambient atmosphere for reproducible ignition.

[13] The voltage rate rise for the .035" diameter Al wire was about .11 v/sec.

H_2O-CO_2 mixtures, and, at 50 torr total pressure in the H_2O-O_2 mixtures. As the wire was heated, near the center of the wire the metal melted and the wire broke. The wire glowed only slightly if at all. A blue-green-white spark was observed at the break, but no flame propagated. The wire retained its metallic luster in all cases. As is seen in Table 15, the averaged data for atmospheres not containing oxygen is essentially equivalent.

In H_2O-O_2 mixtures at 100 and 200 torr total pressure, the wire glowed quite brightly before it broke. The current flowing through the sample went through a maximum, decreased, and again began to increase; in previous work this transition was attributed to the melting of the metal. The higher total resistance at breaking shown in Table 2 also indicates that a higher mean temperature was reached in these experiments. No ignition, however, was ever observed. Although the sample retained its metallic luster, a greater length of the wire appeared to have melted. Photographs of the various products of reaction are shown in Fig. 12. An unreacted piece of wire and a centimeter scale (mm divisions) are included for comparison.

These results are interpreted as follows: in atmospheres not containing O_2 the surface film formed during the ohmic heating was not sufficiently thick to support the molten metal. When the wire broke and exposed molten metal, the mean metal temperature was below the critical temperature of aluminum ($1000^{\circ}C$ as measured by Grosse and Conway) and thus ignition could not occur. Since the breaking spark was observed in pure Ar, it is thought to be an electrical effect, even though the current decreased to zero continuously at the break.

In O_2 containing atmospheres, a similar explanation applies, except that a higher mean temperature was attained due to the higher oxidation rate in the presence of oxygen. The critical temperature was not exceeded, however.

3. The Ignition and Combustion of Magnesium

Experiments were performed in various H_2O mixtures discussed in the aluminum section of this report with unanodized magnesium ribbon of .29 cm average width. The voltage rate rise used was approximately .106 v/sec.

It is shown in Table 2 that the ignition temperature of bulk magnesium samples in O_2 and in H_2O are slightly below the metal melting point (650°C), whereas those in CO_2 are considerably above the metling point. Thus in our experimental apparatus, in which the sample must support itself to maintain ohmic heating, some irreproducibility in ignition would be expected in O_2 and H_2O atmospheres and ignition in CO_2 atmospheres would be expected to be difficult or even impossible[14]. Previous experimental work in O_2-Ar, O_2-CO_2, and CO_2-Ar mixtures has borne out these expectations as do the present experiments as is shown in Table 16, giving the ignition reproducibility for magnesium in the various H_2O mixtures.

In H_2O-O_2 mixtures the ribbon generally ignited before it broke[15]. The ignition (and combustion) flames appeared to be white. Burnign rates were extremely rapid: the 9 cm length exposed to the atmosphere was entirely consumed in less than one second. A photograph of the pehnomenon is shown in Fig. 13 (50%H_2O-50%O_2, total pressure 200 torr). Little if any flame structure is apparent, although the size of the flame suggests that events are occurring in the vapor phase. The dark circle in the photograph is the chamber window, of 1" diameter. Flame spectra revealed no significant difference from the previously attained Mg in O_2-Ar spectrum.

The only recoverable products of combustion were a few white flakes of several mm^2 area and a great deal of grey-white smoke found on the electrodes and top of the chamber as is shown in Fig. 14.

In H_2O-Ar mixtures ignition also occurred before the break. Beautifully colored vapor-phase flames were observed, usually either blue, green or purple, or combinations of these. However, these flames were extremely dim. Two exposures of flames at the same ambient conditions are presented in Fig. 15 (pure H_2O at 100 torr); these differed in camera shutter speed by a factor of five.

Burning times were longer than in H_2O-O_2 mixtures; in particular, at, and only at 50%H_2O-50%Ar and a pressure of

---

[14] Experimental work by Darras, Baque, and Leclercq (Comptes Rendus Acad. Sci., Paris, 249, 1647 (1959) has shown that in even slightly humid CO_2 the Mg ignition temperature is lowered considerably and becomes on the order of the Mg melting point. Thus in the 50%H_2O-50%CO_2 mixtures used in the present investigation some ignitions would be expected.

[15] The averaged experimental data for magnesium is presented in Table 17.

100 torr, the burning persisted for 10 to 15 sec. These flames were observed to consist of two colored zones, the inner blue-green (perhaps MgO) and the outer purple (perhaps MgOH). The long burning time occurred under these conditions each time that the sample was successfully ignited. No explanation can be offered for this abnormally long burning time. Flame spectra obtained at this data point revealed only the Na D lines and complex bands in the 3700-3900 Å region which are due to either $(MgO)_n$ or MgOH.[16] The dimness of the flames was such that only poor spectral plates could be obtained; thus definite identification is difficult.

The products of combustion consisted of large white flakes which resembled the original ribbon shape (Fig. 14). White smoke was also found.

On those few occasions in H_2O-CO_2 mixtures when ignition occurred, the flames were of short duration and resembled the H_2O-Ar flames. Black areas were present on the large white flakes, but the products in all mixtures consisted only of MgO.

In all the gas compositions, on those experiments at which ignition did not occur, the ribbon was twisted and blackened near its center where it had broken. A green spark was seen when the ribbon broke.

4. The Ignition and Combustion of Molybdenum

An experimental investigation of the ignition and combustion of molybdenum at the same data points used in the tantalum investigation is now in progress. That portion of the investigation in the dry gas combinations has been completed and will be described here.

11 cm lengths of 99.95% Mo wire of .035" diameter were obtained from A.D. MacKay, Inc. According to the supplier, the major impurity is tungsten. The wires were mounted in the "L" configuration and heated ohmically with a voltage rise rate of approximately .118 v/sec.

MoO_3 is the major product of the Mo-O_2 reaction at low temperatures. This oxide melts at 795 °C and boils at

[16] Pearse, R.W.B., and Gaydon, A.G., The Identification of Molecular Spectra, Third Edition, Wiley, New York, 1963.

1100°C at 1 atm. Other oxides exist in various temperature ranges which are not well-defined. The metal melts at 2620°C and boils at 5550°C.[17] Thus according to the vapor-phase combustion criterion based on MoO_3, Mo cannot ignite or burn in the vapor phase.

Four basic reaction regimes were observed in the dry gas combinations. Regime one was observed in pure O_2, 50%O_2-50%Ar, and 50%O_2-50%CO_2 at all pressures investigated. As the wire was heated it attained a dull red glow. Near the center of the wire a white hot solid-phase ignition zone developed and spread toward the electrodes before the wire broke. Eventually the wire cross section was consumed; the surface of the wire rippled and drops fell to the bottom of the chamber.

Before ignition occurred, a bright-dark interface was observed to start at the center of the wire and move toward the electrodes. Slightly later a non-luminous condensation zone appeared a few mm to a cm away from the wire, the stand-off distance decreasing with increasing total pressure. This phenomenon is taken to be the melting or boiling of the surface coating of MoO_3 which then recondenses in the decreasing temperature field surrounding the wire. The condensation zone underwent a laminar to turbulent transition and moved away from the wire as the temperature of the wire increased and ignition occurred.

Examples of the bright-dark interface are shown in Fig. 16; the interface is indicated with an arrow in each photograph. The laminar-turbulent transition is depicted in Fig. 17: the top photograph was taken early in the heating period; the middle, midway in the heating period; the white ignition zone is seen in the bottom picture. All of the photographs were taken in 1 atm of O_2 with back illumination so that the condensation zone could be seen.

Example of the white solid-phase combustion are shown in Fig. 18. The turbulent condensation zone is visible due to scattered light.

At the lower pressures in regime one as the flame was extinguishing, growth of a coral-like deposit was observed near the electrodes. The wire which remained was shiny and metallic, whereas the as-received wire was a dull grey color; this fact

[17] Kubaschewski, O., and Hopkins, B.E., Oxidation of Metals and Alloys, Second Edition, Butterworths, London, 1962.

further indicates that the MoO_3 had vaporized during the experiment. This phenomenon did not occur at higher pressures because there the combustion zone receded completely to the electrodes.

At all pressures the chamber was filled with white-green-yellow smoke which was found by X-ray diffraction to be composed of Mo_9O_{26}, MoO_3, and traces of η-MoO_3.[18] Pieces found on the bottom of the chamber which had fallen from the wire consisted of Mo, MoO_2, and traces of MoO_3, as did the coral-like deposits found at the lower pressures. MoO_2 is formed preferentially above 1780°C in Mo oxidation.[17] Typical products of combustion are shown in Fig. 19.

Spectra taken of the white combustion process showed only continuum emission in the wavelength range 3700 to 7400 Å. Both Mo and MoO radiate in this spectral region. Apparently then, regime one is a solid-phase reaction.

Data reduction for Mo in dry gas combinations is shown in Table 18. The power at ignition and at breaking and burning time decreased with increasing pressure as the reaction rate and thus chemical heat release increased.

At 1 atm of pure O_2 the average time between ignition and breaking was .40 sec. A few self-sustained experiments were performed in which the electrical power input was stopped .40, .28, and .14 sec after ignition. The usual combustion mechanism was observed in all cases.

That ignition occurs after the oxide melts is consistent with the results of other investigators and with the ignition criterion (see Table 7). Unfortunately, unforeseen difficulties encountered in the construction of a two-color temperature measuring device have prevented measurement of ignition temperatures in the wire-burning apparatus.

Other authors have observed a combustion mechanism similar to that described above for Mo. Harrison and Yoffee[19] investigated the combustion of Mo wires of .2 mm (.05") diameter suspended vertically and ignited at the lower end in mixtures of O_2-N_2 at 1 atm and in pure O_2 at several pressures. They observed the combustion mechanism described above and also concluded that it is a solid-phase reaction.

[18] Mo_9O_{26} exists from temperatures of 600 to 750°C. Above 750°C, $Mo_9O_{26} \rightarrow Mo_9O_{26}$(M) (ASTM card index).

[19] Harrison, P.L., and Yoffee, A.D. (1961), Proc. Roy. Soc. 261A, 357.

In a recent paper, Bartlett[20] also observed the solid-phase combustion mechanism with the non-luminous condensation zone in an experimental apparatus almost equivalent to that used in this laboratory. However, the diameter of the samples used was approximately four times that of our samples. Since the electrical heating terminates when the metallic cross-section is consumed, it would be expected that Bartlett's samples could attain a higher mean temperature during the heating process.

Bartlett reports that if the metal surface temperature exceeded about 1900°C during the solid-pahse combustion described above, a new reaction mechanism was observed involving a sub-oxide vapor-phase diffusion flame. In this regime the condensation zone was so bright that it almost completely obscured the incandescent Mo rod.

Bartlett associates the 1900°C temperature with that temperature at which preferential oxidation of Mo to MoO_2 rather than MoO_3 occurs and argues that polymerization reactions are strongly exothermic in the system; thus he can postulate the following combustion mechanism: the initial step occurs on the surface

$$Mo + O_2 \longrightarrow MoO_2(g).$$

The strongly exothermic reaction which occurs in the gas phase is

$$\frac{3}{2} O_2 + 3\, MoO_2(g) \longrightarrow (MoO_3)_3\ (g)$$

with an energy release of 598 Kcal/mole $(MoO_3)_3$. Thus in this case there is a vapor-phase diffusion flame in which the fuel is the metal suboxide (MoO_2) rather than the metal. Attempts will be made to duplicate this mechanism.

Regime two is the simple melting mechanism which occurred in pure Ar at all pressures investigated. As the wire was heated electrically it continuously approached a white-hot glow; at the higher pressures it then beaded and broke. Occasionally a large piece fell out of the middle of the wire. The condensation zone was observed at all pressures.

---

[20] Bartlett, R.W. (1965), "Molybdenum Oxidation Kinetics at High Temperatures," J. Electrochem. Soc 112, 744-746.

The wire which remained (Fig. 19) was a shiny metallic color and consisted only of Mo. Blue smoke from the condensation zone which had accumulated on the electrode blocks was composed of MoO_3 and η-MoO_3. The averaged data is shown in Table 18: the sample weight loss after an experiment is attributed to the evaporation of the oxide.

Regime three is the designation of the mechanism found in pure CO_2 at 50 torr and in 50%CO_2-50%Ar at 50 and 100 torr (maximum CO_2 partial pressure 50 torr). The sequence of events was exactly that described for regime two except that the smoke found on the electrode blocks was grey-green. X-ray diffraction of this smoke revealed that it consisted of MoO_2, η-MoO_3, Mo_9O_{26}, and traces of Mo_2C. The wire contained traces of MoO_2.

Finally, regime four (pure CO_2 and 50%CO_2-50%Ar mixtures with CO_2 pressure greater than or equal to 300 torr) again was similar to regime two except that the grey-green smoke was found and that the wire surface was a maroon or red-brown color. This surface coating was primarily MoO_2, with traces of MoO_3, MoC, and Mo_2C.

The X-ray diffraction results in all four regimes indicate a significant trend: the high-temperature oxide (MoO_2) was found only on the wire, whereas the smoke formed in the condensation zone consisted only of the low temperature oxides. In regime one in particular this fact is consistent with the solid-phase combustion model (that the highest temperature in the system is attained at or near the surface of the wire).

A few self-sustained experiments were conducted in regime four (pure CO_2 at 1 atm). At the termination of the electrical heating, while the wire was white hot, the wire immediately ceased to glow and did not break. Thus reaction occurring in regime four is merely oxidation.

During the next report period results of an investigation of the effect of H_2O (at the data points used in the Ta, Al, and Mg investigations) will become available.

VI. FUTURE DEVELOPMENTS

The experimental portion of the investigation will be emphasized during the next report period. The Mo-H_2O experiments will be completed and wire-burning experiments will be attempted with Si. Also, the furnace experiments discussed in Section III should commence.

LIST OF REFERENCES FOR EXPERIMENTAL IGNITION TEMPERATURES

(2) Reynolds, W. C. (1959), NASA TN D-182.

(6) Freeman, E. S., and Campbell, C. (1963), Trans. Farad. Soc. 59, 165.

(23) Leibowitz, L.,Baker, L. Schnizlein, J. G., Mishler, L. W., and Bingle, J. B. (1963), Nucl. Sci. Eng. 15 (4), 395.

(24) Leibowitz, L., Schnizlein, J. G., and Mishler, L.W. (1963), Nucl. Sci. Eng. 15 (4), 404.

(28) Grosse, A. V., and Conway, J. B. (1958), Ind. Eng. Chem. 50.,663.

(30) **Schnizlein**, J. G., Baker, L.,and Vogel, R. C. (1960) **ANL-RCV-SL-1781.**

(35) Dean, L. E., and Thompson, W. R. (1961), ARS Journal 31 (7), 917.

(36) Pilling, N. B., and Bedworth, R. E. (1923), J Inst. Met. 29, 529.

(38) Friedman, R., and Macek, A. (1962), Combust. Flame 6, 9.

(39) Friedman, R., and Macek, A. (1963), Ninth Symposium (International) on Combustion, 703, Academic Press, New York.

(40) Hill, P. R., Adamson, D., Foland, D. H., and Bressette, W. E. (1956), NACA RM L55L23b.

(48) Cassel, H. M., and Liebman, I. (1959), Combust. and Flame 3, 467.

(53) Hartmann, I. (1948), Ind. Eng. Chem. 40, 752.

(57) Fassell, W. M., Jr., Gulbransen, L. B., Lewis, J. R., and Hamilton, J. H. (1951), J. Metals 3, 522.

(269) Hayes, E. T., and Roberson, A. H. (1949), Trans. Electrochem. Soc. 96, 142.

(306) Schnizlein, J. G., Porte, H.A., Pizzolato, P. J., Bingle, J.D., Fischer, D.F., Mishler, L.W., Martin, P., and Vogel, R.C. (1958), ANL-5924.

(323) Rhein, R. A., (1964), Fall 1964 Western States Combustion Meeting, Preprint 64-25.

(326) Kuehl, D. K. (1964), Fall 1964 Western States Combustion Meeting, Preprint 64-21.

(330) Rhein, R. A. (1964), JPL Tech. Rep. No. 32-679.

(332) Kuehl, D. K. (1965), AIAA Second Aerospace Sciences Meeting, AIAA Paper No. 65-103.

(333) Jacobson, M., Cooper, A.R., and Nagy, J. (1964), Bureau of Mines Report of Investigations 6516.

(336) Anderson, H.C. and Belz, L. H. (1953), J. Electrochem. Soc. 100, 240.

(339) Baur, J.P., Bridges, D.W., and Fassell, W.M. Jr. (1955), J. Electrochem. Soc. 102, 490.

(341) Macek, A., Friedman, R., and Semple, J. M., (1964) Hetergeneous Combustion, Wolfhard, H. G., Glassman, I., and Green, L., Jr., editors, 3. Academic Press, New York.

(384) Albrecht, W.M., Klopp, W.D., Koehl, B.G., and Jaffee, R.I. (1961), Trans. AIME 221, 110.

(386) Gulbransen, E.A. and Andrew, K.F. (1958), Trans. AIME 212, 281.

(435) Leibowitz, L., Bingle, J.D., and Homa, M. (1964), J. Electrochem. Soc. 111, 248.

(454) Fairbairn, A. (1965), UKAEA AHSB(S)R80.

(465) Cowgill, M.G. and Stringer, J. (1961) Niobium, Tantalum, Molybdenum, and Tungsten, Quarrell, A.G., editor, 190. Elsevier, Amsterdam.

(475) Cassel, H.M. (1964), Bureau of Mines Report of Investigations 6551.

(477) Rhein, R.A., (1965), JPL Space Programs Summary No. 37-31, Vol. IV, 201.

(129) Loriers, J. (1952), Rev. Metall. 49, 801.

(130) Brown, C. R. (1934), The Determination of the Ignition Temperatures of Solid Materials. D. Sc. Thesis, Catholic University of America.

(157) Kubaschewski, O., and Ebert, H. (1947), Z. Metallk. 38, 232.

(173) Cassel, H. M., and Liebman, I. (1963), Combust. Flame 7, 79.

(175) Loriers, J., (1952), Comptes Rendus Acad. Sci., Paris 234, 91.

(177) Hartmann, I., and Nagy, J. (1944), Bureau of Mines Report of Investigations 3751.

(178) Hartmann, I., Nagy, J., and Brown, H.R. (1943), Bureau of Mines Report of Investigations 3722.

(205) Constantinides, G. (1952), Ann. Chim. Roma 42, 383.

(221) Simnad, M., and Spilners, A. (1955), J. Met. 7, 1011.

(231) Schnizlein, J. G., Pizzolato, P. J., Porte, H.A., Bingle, J. D., Fisher, D. F., Misnler, L.W., and Vogel, R. C. (1959), ANL 5974.

(232) Darras, R., Baque, P., and Leclercq, D. (1959), Comptes Rendus Acad. Sci., Paris 249, 1647.

(244) Hartmann, I., Nagy, J., and Jacobson, M. (1951), Bureau of Mines Report of Investigations 4835.

(248) Conway, J. B., and Kirshenbaum, M. S., Ninth Progress Report Contract N9-ONR-87301, Res. Inst. Temple Univ., January 1954.

(250) Tammann, G., and Boehme, W. (1934), Z. anorg. allge. Chem. 217, 225.

(251) Darras, R., Baque, P., and Leclercq, D. (1959), NP-9715.

(261) McIntosh, A. B., and Bagley, K. Q. (1956), J. Inst. Met. 84, 251,

TABLE 1.

ESTIMATED TRANSITION TEMPERATURES

System	T_{trans}, °C	Mechanism
$Al-O_2$	2030	[b]
$Mg-O_2$	450	[e] or [f]
$Mg-CO_2$	550	[e] or [f]
$Ti-O_2$	850	[c]
$Zr-O_2$	900 ± 100	[c] or [f]
$Ta-O_2$	500	[f]
$Mo-O_2$	700	[b] or [f]
$Ca-O_2$	400	[e] or [f]
$Si-O_2$	$1400 < T_{trans} < 1610$	[b] ?
$U-O_2$	250	[d]

TABLE 2.

EXPERIMENTAL IGNITION TEMPERATURES OF MAGNESIUM

ATMOSPHERE	CONDITION	STATED SIZE	IGNITION TEMPERATURE, °C	REFERENCE
AIR	DD[1]		520	(53)
	DD	$< 40\mu$	510	(205)
	QP[2]	$< 53\mu$	478	(333)
	DD	$40 - 66\mu$	551	(205)
	DD	$< 74\mu$	520	(177)
	DD	$< 74\mu$	620	(333)
	QP	$< 74\mu$	490	(333)
	DD	$< 149\mu$	613	(178)
	QP	$< 149\mu$	517	(178)
	QP	$< 149\mu$	520	(333)
		$< 53\mu$	510	(454)
	QP	$< 44\mu$	563	(477)
OXYGEN	B[3]		649	(157)
	B	~ 10 g.	623	(28), (248)
	B		591	(339)
WATER VAPOR	B		635	(157)

[1]Dust Dispersion; [2]Quiescent Pile; [3]Bulk

TABLE 2. (Cont.)

ATMOSPHERE	CONDITION	STATED SIZE	IGNITION TEMPERATURE, °C	REFERENCE
CARBON DIOXIDE	QP	$<44\mu$	749	(323), (330)
	QP	$<53\mu$	630	(333)
	QP	$<149\mu$	630	(178)
	B		642	(261)
	B	1.23 mm^{-1}	880	(232), (251)
	B	1.23 mm^{-1}	920	(232), (251)
	QP	$<74\mu$	600	(333)
NITROGEN	QP	$<53\mu$	575	(333)
	QP	$<74\mu$	550	(333)
	QP	$<149\mu$	520	(333)
	QP	$<149\mu$	530	(178)

TABLE 3

EXPERIMENTAL IGNITION TEMPERATURES FOR TITANIUM

ATMOSPHERE	CONDITION	STATED SIZE	IGNITION TEMPERATURE, °C	REFERENCE
AIR	DD		480	(53)
	DD	<40 μ	401	(205)
	QP	<44 μ	480	(333)
	QP	<44 μ	470	(333)
	DD	40-53 μ	425	(205)
	DD	<66 μ	412	(205)
	QP	<74 μ	460	(333)
	DD	<149 μ	480	(178)
	QP	<149 μ	460	(178)
	QP	1-5 μ	625	(477)
OXYGEN	B	2.25 to 7.88 mm^{-1}	815	(35)
CARBON DIOXIDE	QP	<44 μ	900	(333)
	QP	<44 μ	470	(333)
	QP	<74 μ	680	(333)

TABLE 3. (Cont.)

ATMOSPHERE	CONDITION	STATED SIZE	IGNITION TEMPERATURE, °C	REFERENCE
CARBON DIOXIDE	QP	$<149\mu$	680	(178)
	QP	1200 - 6000 mm^{-1}	670	(323), (330)
	QP	445 mm^{-1}	550	(244)
	B	2.25 to 7.88 mm^{-1}	1520	(35)
NITROGEN	QP	$<44\mu$	900	(333)
	QP	$<44\mu$	500	(333)
	QP	$<74\mu$	900	(333)
	QP	445 mm^{-1}	760	(244)
	QP	1200 - 6000 mm^{-1}	830	(323), (330)

TABLE 4.

EXPERIMENTAL IGNITION TEMPERATURES FOR URANIUM

ATMOSPHERE	CONDITION	STATED SIZE	IGNITION TEMPERATURE, °C	REFERENCE
AIR	B		397	(23)
	B		380	(24)
	B		330	(24)
	QP	74	145	(477)
CARBON DIOXIDE	QP	$<74\mu$	235	(323), (330)
	DD	556 mm^{-1}	560	(244)
	QP	556 mm^{-1}	350	(244)
	B	.9 mm^{-1}	800	(251)
NITROGEN	QP	$<74\mu$	357	(323), (330)
	QP	556 mm^{-1}	410	(244)
OXYGEN			300	(435)

TABLE 5.

EXPERIMENTAL IGNITION TEMPERATURES FOR CALCIUM

ATMOSPHERE	CONDITION	STATED SIZE	IGNITION TEMPERATURE, °C	REFERENCE
AIR	B	.227-.25 mm^{-1}	730	(2)
	QP	<44μ	229	(477)
OXYGEN	B	~10 g.	550	(28), (248)
	B		550	(36)
CARBON DIOXIDE	QP	<44μ	293	(323), (330)
NITROGEN	QP	<44μ	327	(323), (330)
	QP	<44μ	360	(323), (330)
	QP	<44μ	671	(323), (330)

TABLE 6.

EXPERIMENTAL IGNITION TEMPERATURES FOR TANTALUM

ATMOSPHERE	CONDITION	STATED SIZE	IGNITION TEMPERATURE, °C	REFERENCE
AIR	DD	$< 44\mu$	630	(333)
	QP	$< 44\mu$	300	(333)
OXYGEN	B	.845 mm^{-1}	1300	(384)
	B	4.2 mm^{-1}	1000	(465)

TABLE 7.

EXPERIMENTAL IGNITION TEMPERATURES FOR MOLYBDENUM

ATMOSPHERE	CONDITION	STATED SIZE	IGNITION TEMPERATURE, °C	REFERENCE
AIR	DD	$< 74\mu$	720	(333)
	QP	$< 74\mu$	360	(333)
OXYGEN	B	$\sim 10g.$	750	(28), (248)
	B		725	(339)
	B	2.33 mm^{-1}	750	(221)

TABLE 8.

EXPERIMENTAL IGNITION TEMPERATURES FOR ZIRCONIUM

ATMOSPHERE	CONDITION	STATED SIZE	IGNITION TEMPERATURE, °C	REFERENCE
AIR	DD		25	(53)
	QP	$<44\mu$	210	(333)
	DD	$<149\mu$	25	(178)
	QP	$<149\mu$	210	(178)
	DD	2000 mm^{-1}	20	(244), (333)
	QP	2000 mm^{-1}	220	(244)
	QP	2000 mm^{-1}	190	(244), (333)
	QP	1035 mm^{-1}	192	(336)
	QP	1017 mm^{-1}	181	(336)
	QP	985 mm^{-1}	181	(336)
	QP	909 mm^{-1}	181	(336)
	QP	883 mm^{-1}	186	(336)
	QP	330 mm^{-1}	300	(244), (333)
	DD	330 mm^{-1}	350	(244)
	QP	2000 mm^{-1}	193	(477)
OXYGEN	B	15.05 mm^{-1}	820	(306)
	B	1.41 mm^{-1}	1000	(269)
			800	(386)

TABLE 8. (Cont.)

ATMOSPHERE	CONDITION	STATED SIZE	IGNITION TEMPERATURE, $^{\circ}$ C	REFERENCE
CARBON DIOXIDE	QP	$<44\mu$	560	(333)
	QP	$<149\mu$	560	(178)
	QP	2000 mm^{-1}	365	(323), (330)
	QP	2000 mm^{-1}	620	(244), (333)
	DD	1820 mm^{-1}	650	(244)
	QP	330 mm^{-1}	710	(244), (333)
NITROGEN	QP	$<44\mu$	530	(333)
	QP	$<149\mu$	530	(178)
	QP	2000 mm^{-1}	508	(323), (330)
	QP	2000 mm^{-1}	790	(244), (333)

TABLE 9.

EXPERIMENTAL IGNITION TEMPERATURES FOR ALUMINUM

ATMOSPHERE	CONDITION	STATED SIZE	IGNITION TEMPERATURE, °C	REFERENCE
AIR	DD		645	(53)
	DD	$<44\mu$	650	(333)
	QP	$<44\mu$	760	(333)
	QP	$<44\mu$	900	(333)
	DD	$<74\mu$	645	(177)
	QP	$<74\mu$	490	(333)
	DD	$<149\mu$	673	(178)
	QP	$<149\mu$	585	(178)
	QP	300,000 mm^{-1}	538	(477)
OXYGEN	B	7.8 mm^{-1}	2030	(326), (332)
CARBON DIOXIDE	QP	$<44\mu$	900	(333)
	QP	$<74\mu$	540	(333)
	QP	$<149\mu$	655	(178)
	QP	706 mm^{-1}	390	(323), (330)
	QP	200,000 mm^{-1}	390	(323), (330)

TABLE 9. (Cont.)

ATMOSPHERE	CONDITION	STATED SIZE	IGNITION TEMPERATURE, °C	REFERENCE
NITROGEN	QP	$<44\mu$	750	(333)
	QP	$<74\mu$	800	(333)
	QP	$<149\mu$	725	(178)
CO_2-N_2-H_2O	SP[4]	$171mm^{-1}$	2030	(38)
CO_2-N_2	SP	$171mm^{-1}$	2030	(39)

TABLE 10.

EXPERIMENTAL IGNITION TEMPERATURES FOR SILICON

ATMOSPHERE	CONDITION	STATED SIZE	IGNITION TEMPERATURE, °C	REFERENCE
AIR	QP	$<53\mu$	950	(333)
	QP	$<74\mu$	790	(333)
	QP	$<149\mu$	950	(178)
	DD	$<149\mu$	775	(178)

[4]Single particle

TABLE 10. (Cont.)

ATMOSPHERE	CONDITION	STATED SIZE	IGNITION TEMPERATURE, °C	REFERENCE
CARBON DIOXIDE	QP	$<53\mu$	1000	(333)
	QP	$<149\mu$	1000	(178)
NITROGEN	QP	$<53\mu$	1000	(333)
	QP	$<149\mu$	1000	(178)

TABLE 11.

EXPERIMENTAL IGNITION TEMPERATURES FOR LITHIUM

ATMOSPHERE	CONDITION	STATED SIZE	IGNITION TEMPERATURE, °C	REFERENCE
OXYGEN	B	~ 10 g.	190	(28), (248)
CARBON DIOXIDE	QP	$<100\mu$	330	(323), (330)
NITROGEN	QP	$<100\mu$	399	(323), (330)
AIR	QP	100	374	(477)

TABLE 12.

EXPERIMENTAL IGNITION TEMPERATURES FOR BERYLLIUM

ATMOSPHERE	CONDITION	STATED SIZE	IGNITION TEMPERATURE, °C	REFERENCE
AIR	DD	6000 mm^{-1}	910	(333)
	QP	6000 mm^{-1}	540	(333)
		37	635	(454)
		500-1676	780	(454)
	QP	.1	20	(477)
H_2O-CO_2-N_2-HCl-O_2	SP	158mm^{-1}	2377	(341)

Table 13.

Results of X-Ray Diffraction Analysis of Tantalum Reaction Products

Regime and Gas Composition	Major Specie Present	Minor Species Present
1, O_2-Ar	α- + β-Ta_2O_5*	
O_2-CO_2	α-Ta_2O_5	β-Ta_2O_5
2, O_2-Ar	α- + β-Ta_2O_5	
O_2-CO_2	α- + β-Ta_2O_5	
CO_2-Ar	α-Ta_2O_5 + TaC	β-Ta_2O_5
3	α- + β-Ta_2O_5	
4	α-Ta_2O_5	β-Ta_2O_5
H_2O-O_2	α-Ta_2O_5	β-Ta_2O_5
H_2O-CO_2	α- + β-Ta_2O_5	
H_2O-Ar	α- + β-Ta_2O_5	
Smoke found after Ar melt	β-Ta_2O_5	α-Ta_2O_5

* β-Ta_2O_5 is the allotropic form of Ta_2O_5 below 1360°C and α-Ta_2O_5 is that above 1360°C (ASTM Card Index).

TABLE 14.

AVERAGED EXPERIMENTAL DATA FOR TANTALUM

Reaction Regime	Initial Sample Weight, mg	Recovered Sample Weight, mg	Total Power, Watts			Total Resistance, ohms			Total Burning Time, Sec
			at Ignition	at Breaking	at I_{max}	at Ignition	at Breaking	at I_{max}	
1 O_2-Ar	839.0	904.0	60.0	38.2	-----	.143	.344	-----	5.4
O_2-CO_2	833.0	875.3	56.4	17.5	-----	.134	.729	-----	8.7
2 Overall	838.0	891.0	----	43.6	110.0	-----	5.70	.167	-----
O_2-Ar	836.0	955.0	----	----	66.2	-----	----	.150	-----
O_2-CO_2	837.0	945.0	----	27.0	67.2	-----	1.09	.146	-----
CO_2-Ar	839.0	911.0	----	28.1	131.9	-----	7.06	.177	-----
3 Overall	839.0	944.0	52.9	19.3	-----	.139	1.04	----	11.8
O_2-Ar	840.0	958.0	50.5	16.1	-----	.140	1.23	----	12.1
O_2-CO_2	837.6	930.1	59.2	22.1	-----	.140	.793	----	10.9
4	838.5	900.0	----	344.2	302.5	----	.444	.263	-----
pure Ar	840.0	833.0	----	465.0	-----	----	.250	----	-----

Reaction Regime	Initial Sample Weight, mg	Recovered Sample Weight, mg	Total Power, Watts			Total Resistance, ohms			Total Burning Time, Sec
			at Ignition	at Breaking	at I_{max}	at Ignition	at Breaking	at I_{max}	
$H_2O - O_2$	834.0	891.0	79.4	28.8	-----	.171	.860	----	7.1
H_2O-CO_2	833.0	932.0	----	----	133.1	----	----	.189	-----
H_2O-Ar	832.0	925.0	-----	----	126.3	----	----	.189	-----
(1)*	838.0	945.5	83.1	----	-----	.173	-----	-----	11.5
(2, CO_2-Ar)*	840.1	897.1	----	----	124.5	-----	-----	.164	-----

TABLE 14. (cont.)

TABLE 15.

AVERAGED EXPERIMENTAL DATA FOR ALUMINUM

Reaction Regime	Initial Sample Weight, mg	Recovered Sample Weight, mg	Total Power at Breaking, watts	Total Resistance at Breaking, ohms
H_2O-O_2	184.9	184.5	59.5	.0359
H_2O-CO_2	185.0	185.0	45.8	.0237
H_2O-Ar	185.2	185.2	44.4	.0234
pure Ar	185.4	185.4	44.8	.0239

TABLE 16.

REPRODUCIBILITY OF MAGNESIUM IGNITION

Atmosphere Composition	Total Pressure, mm Hg	Number of Experiments	% Ignited
Pure H_2O	50	5	60
	100	5	80
50% H_2O-50% Ar	50	5	60
	100	16	75
	200	5	20
50% H_2O-50% O_2	50	7	71
	100	8	88
	200	3	100
50% H_2O-50% CO_2	50	5	40
	100	5	0
	200	5	0

TABLE 17.

AVERAGED EXPERIMENTAL DATA FOR MAGNESIUM

Reaction Regime	Initial Sample Weight, mg	Recovered Sample Weight, mg	Total Power, Watts		Total Resistance, ohms		Total Burning Time, Sec.
			at Ignition	at Breaking	at Ignition	at Breaking	
H_2O-O_2	80.2	41.7	17.7	18.4	.080	.078	.808
H_2O-CO_2	86.4	85.8	----	21.8	----	.076	----
H_2O-Ar	84.1	72.4	23.3	16.2	.050	.157	4.35

TABLE 18.

AVERAGED EXPERIMENTAL DATA FOR MOLYBDENUM

Reaction Regime	Initial Sample Weight, mg	Recovered Sample Weight, mg	Total Power, Watts		Total Resistance, ohms		Total Burning Time, sec
			at Ignition	at Breaking	at Ignition	at Breaking	
1 Overall	685.6	567.1	50.3	35.4	.073	.238	6.37
1 O_2-Ar	685.1	552.6	47.1	33.3	.072	.231	5.90
1 O_2-CO_2	686.6	607.5	56.5	40.4	.075	.256	7.75
2	682.2	668.5	———	287.6	———	.116	———
3	683.2	611.7	———	218.6	———	.141	———
4	685.1	676.6	———	193.3	———	.119	———

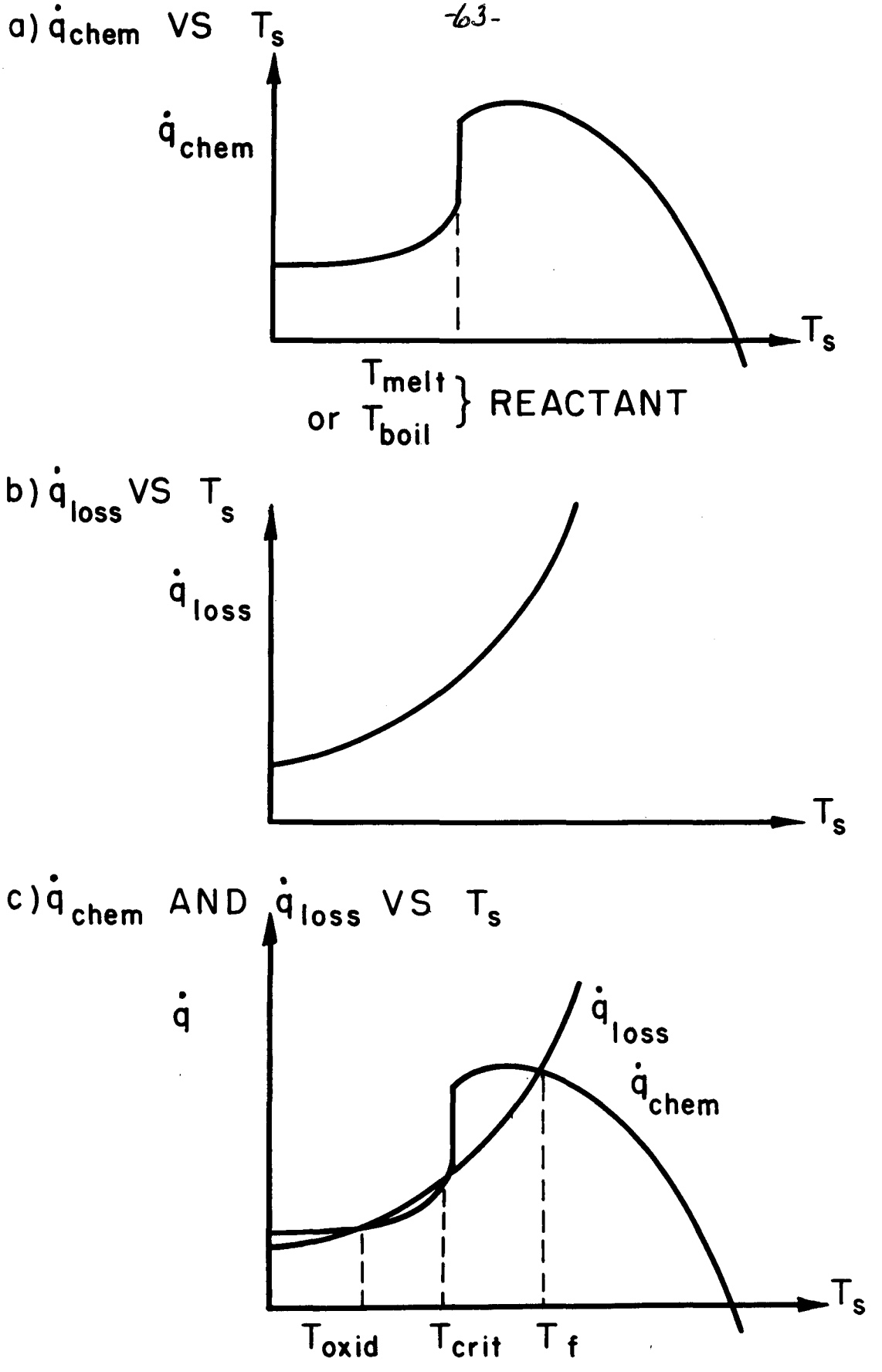

RATE OF CHEMICAL ENERGY RELEASE AND RATE OF HEAT LOSS VS SURFACE TEMPERATURE

FIGURE 1

a - NO SOLID-PHASE PRODUCT

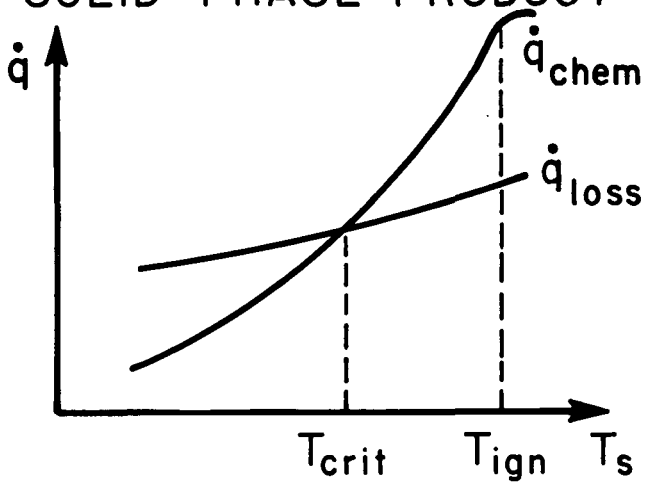

b - $T_{trans} < T_{crit}$

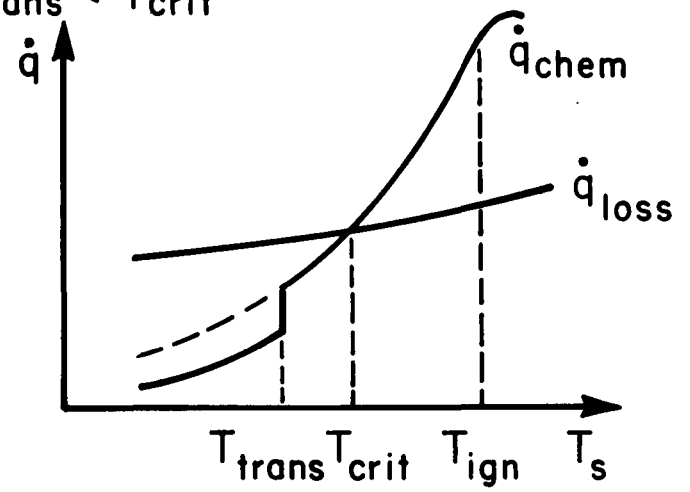

c - $T_{trans} > T_{crit}$

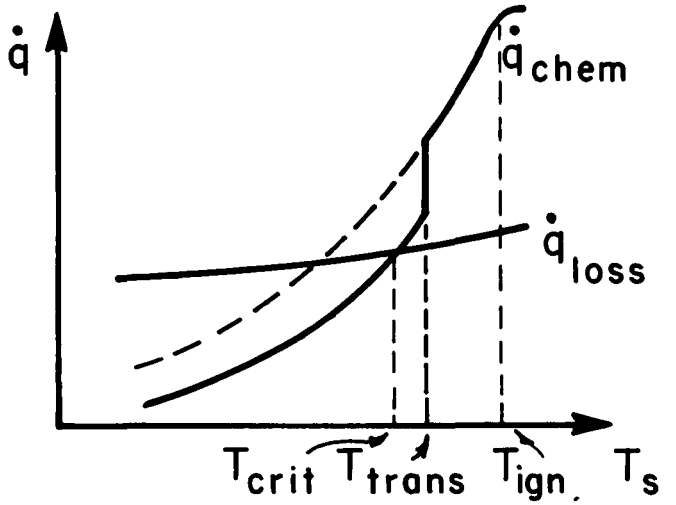

THE IGNITION CRITERION

FIGURE 2

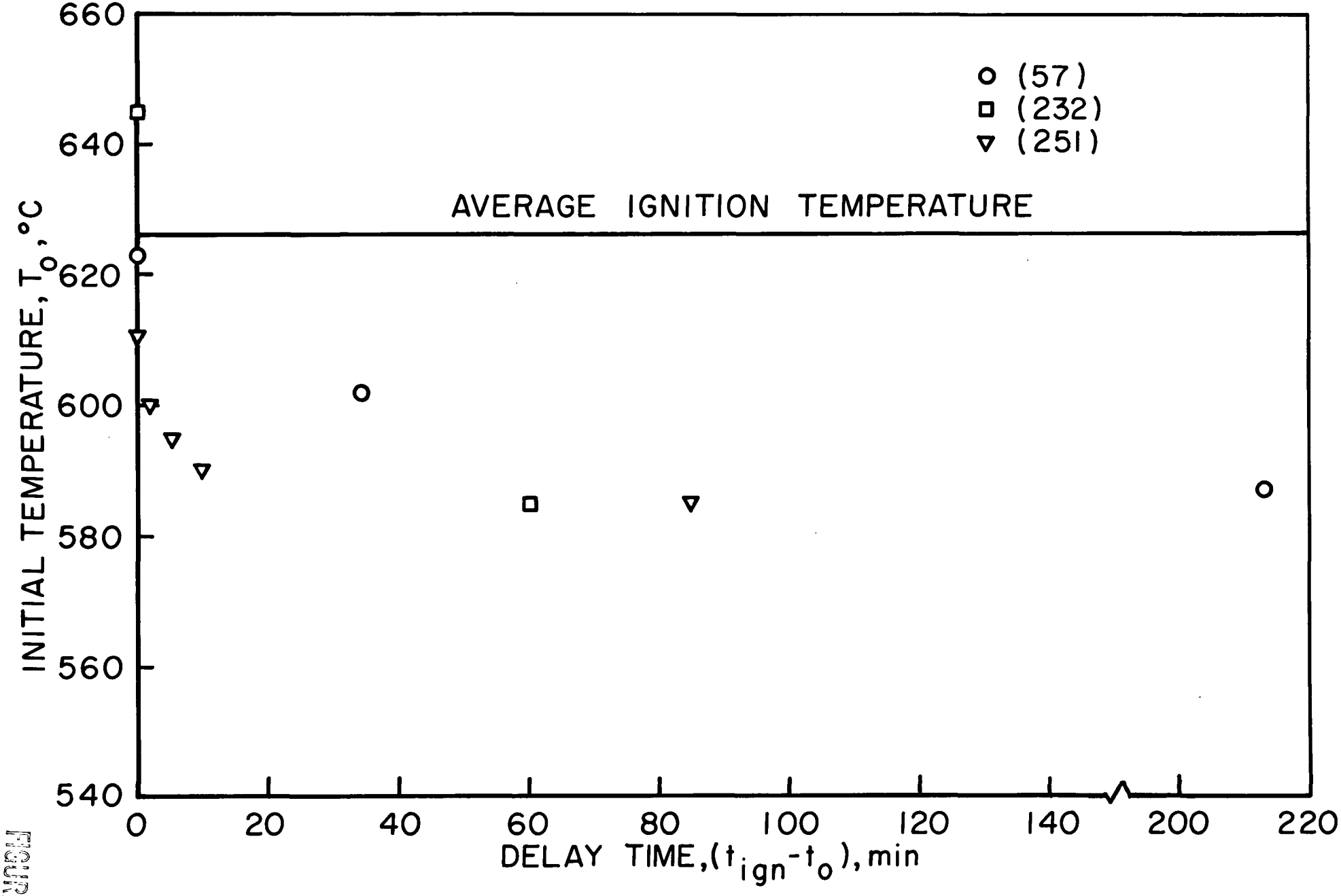

FIGURE 8

INITIAL TEMPERATURE vs DELAY TIME: BULK MAGNESIUM IN OXYGEN OR AIR

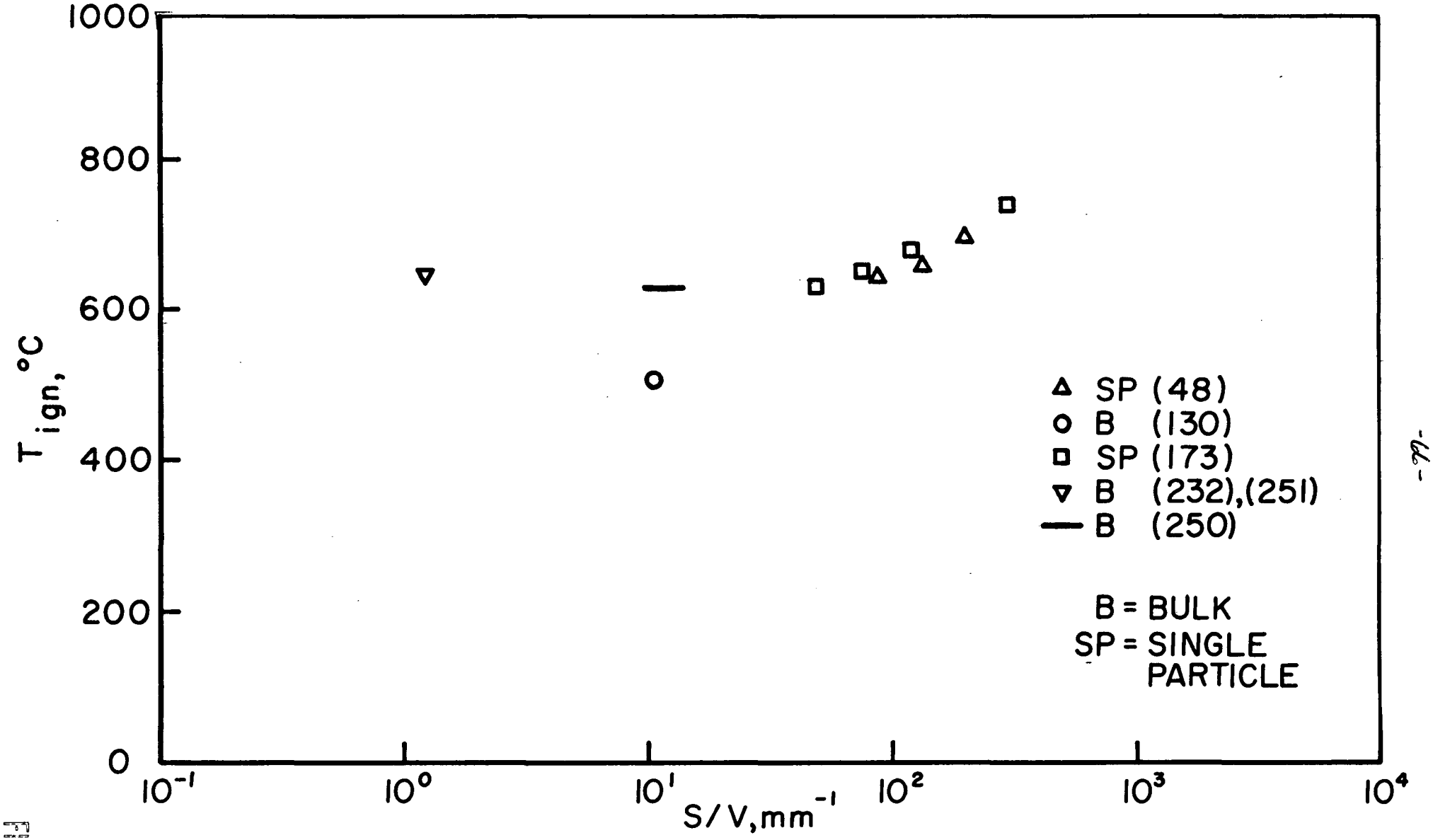

FIGURE 4

IGNITION TEMPERATURE vs SURFACE - VOLUME RATIO: MAGNESIUM IN AIR

AP29-4001-65

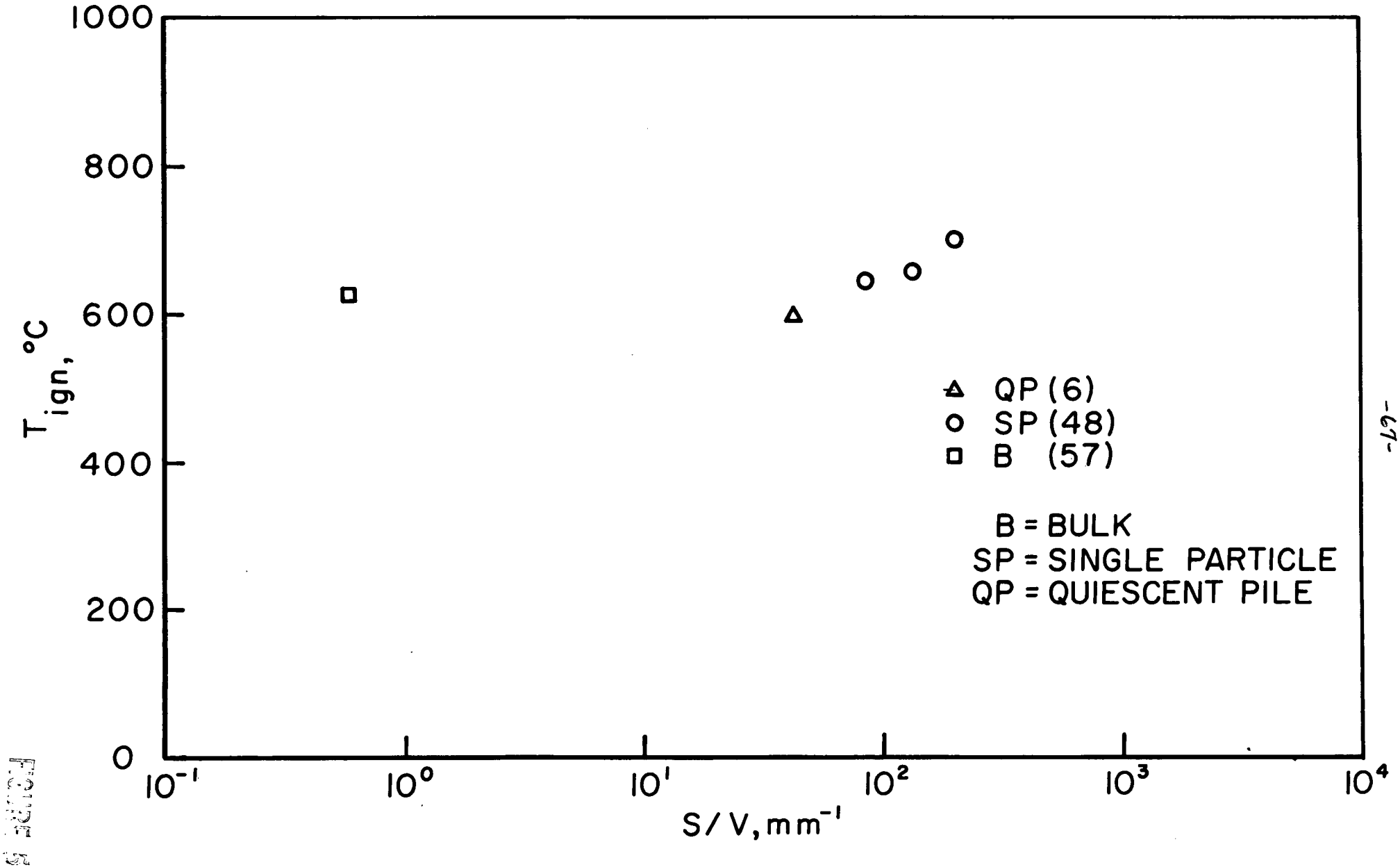

IGNITION TEMPERATURE vs SURFACE-VOLUME RATIO: MAGNESIUM IN OXYGEN

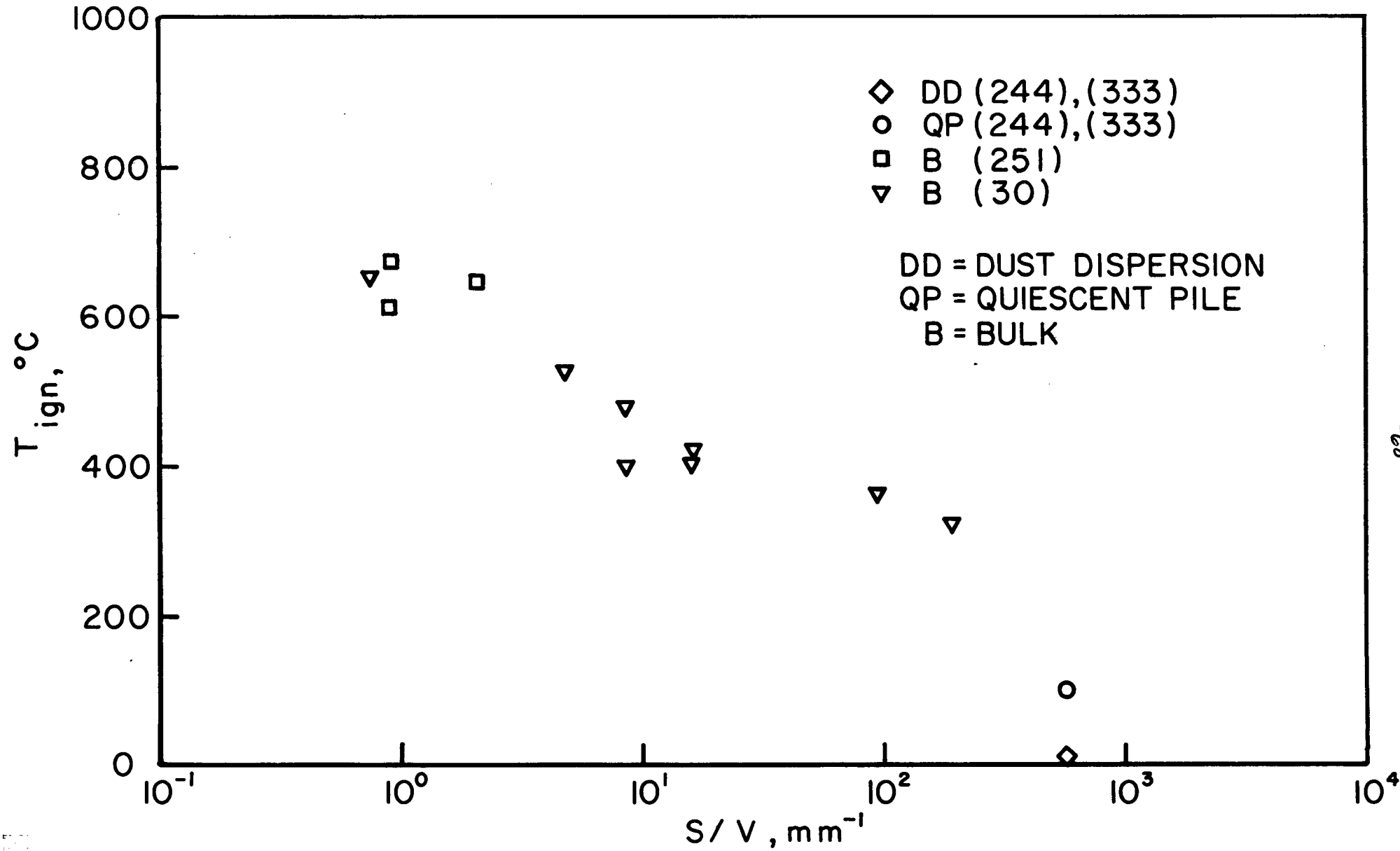

IGNITION TEMPERATURE vs SURFACE-VOLUME RATIO: URANIUM IN AIR

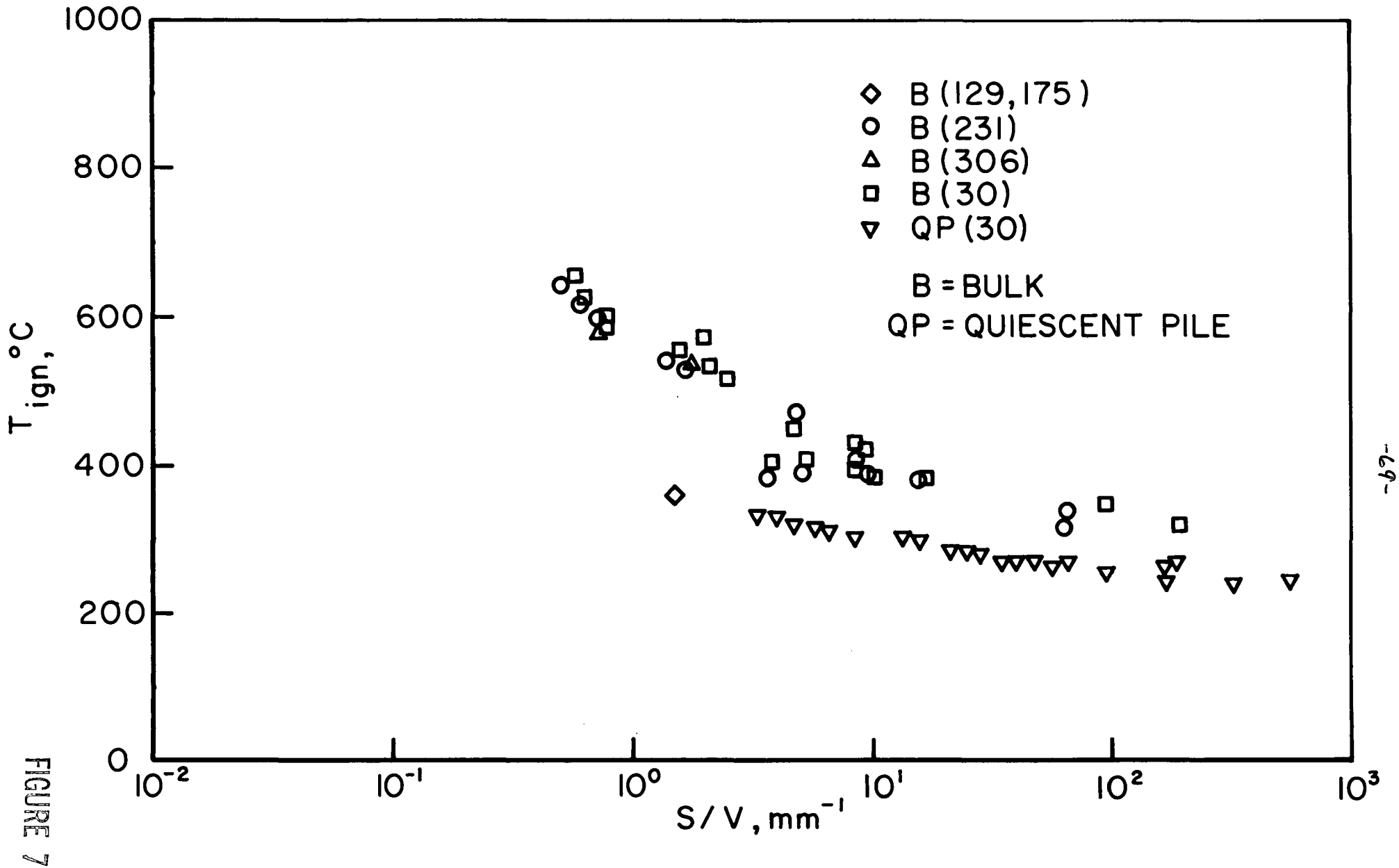

FIGURE 7

IGNITION TEMPERATURE vs SURFACE-VOLUME RATIO: URANIUM IN OXYGEN

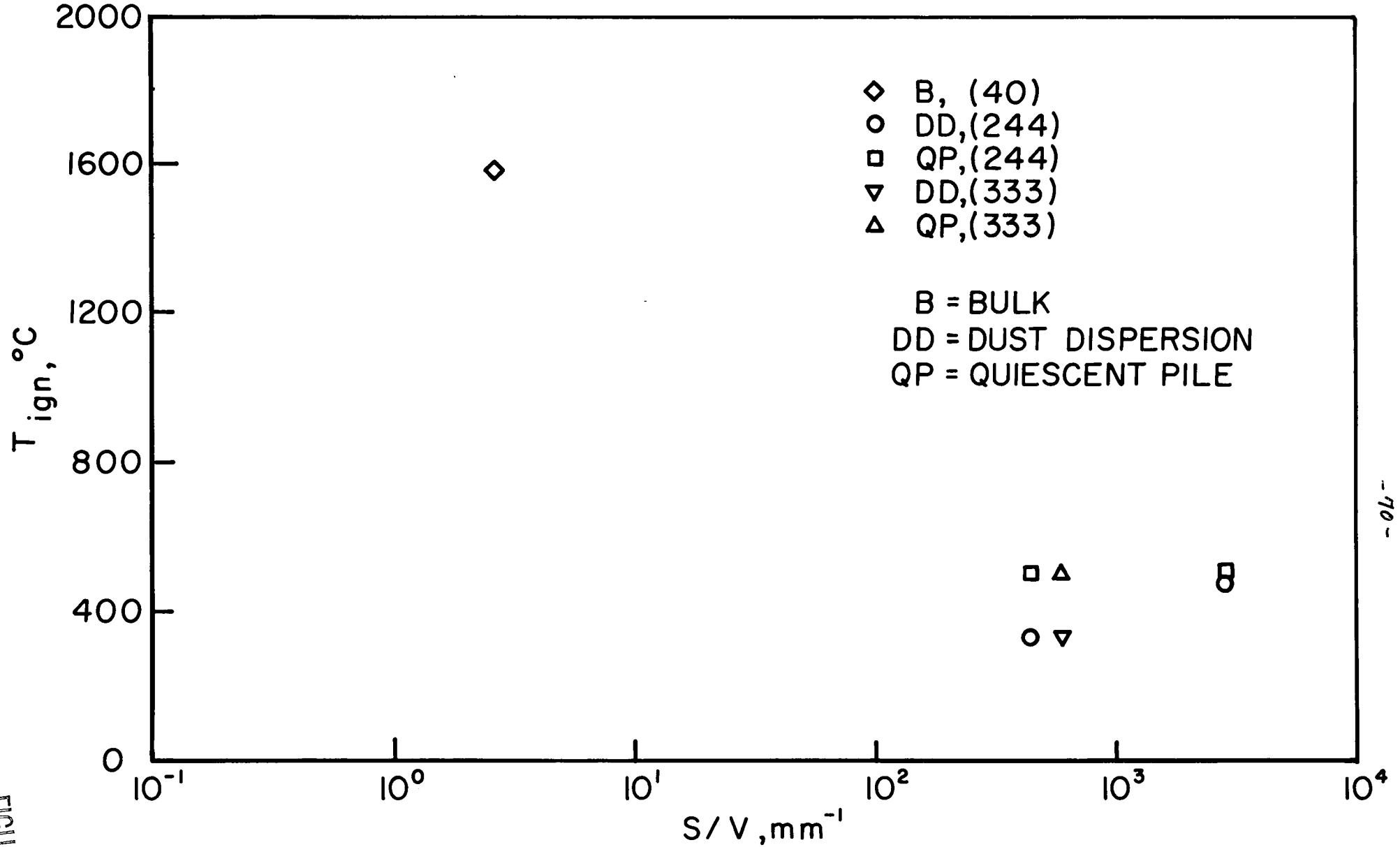

FIGURE 8

IGNITION TEMPERATURE vs SURFACE-VOLUME RATIO: TITANIUM IN AIR

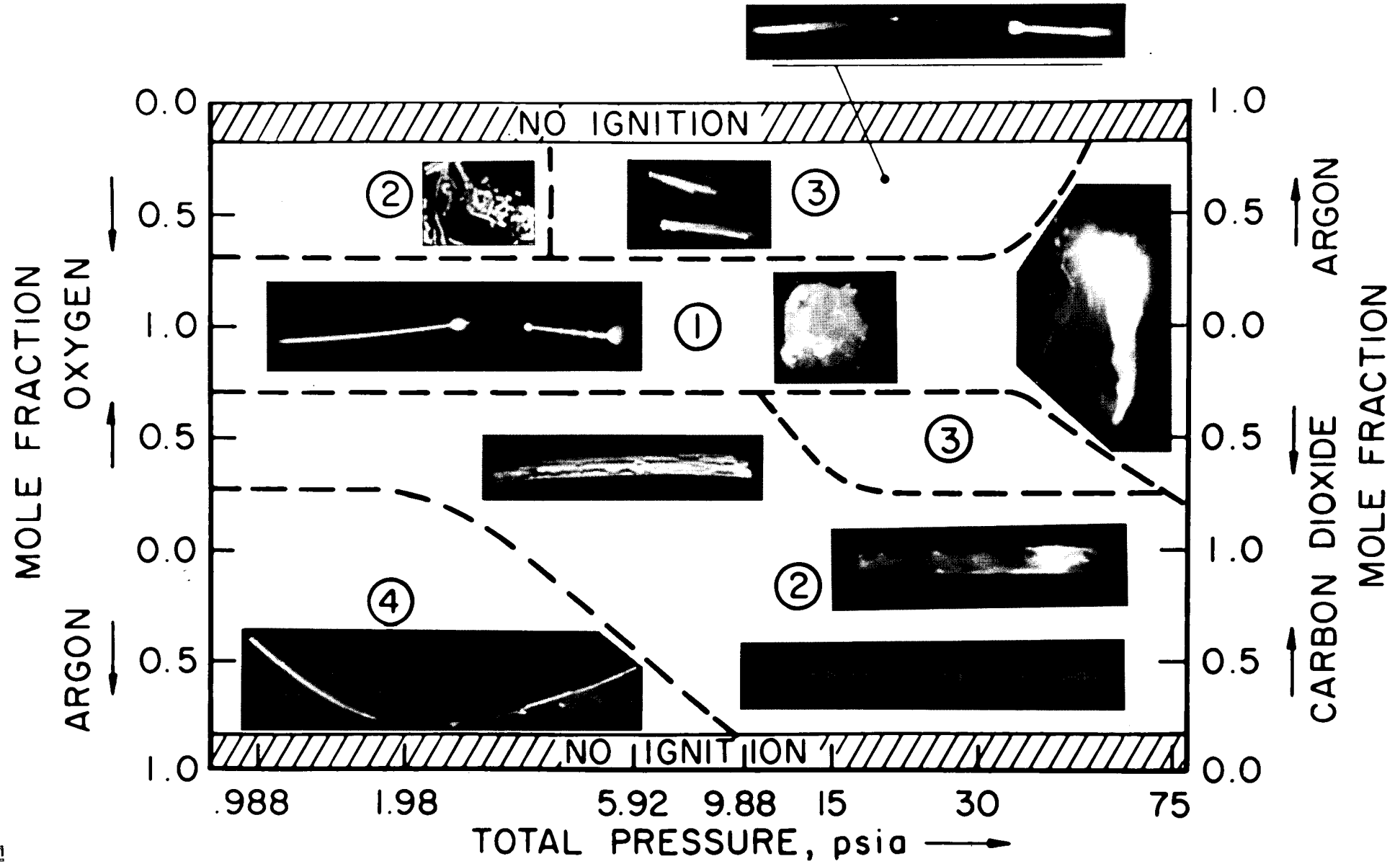

FIGURE 9

REACTION REGIMES OF TANTALUM WIRE IN
O_2 - Ar, O_2 - CO_2 AND CO_2 - Ar

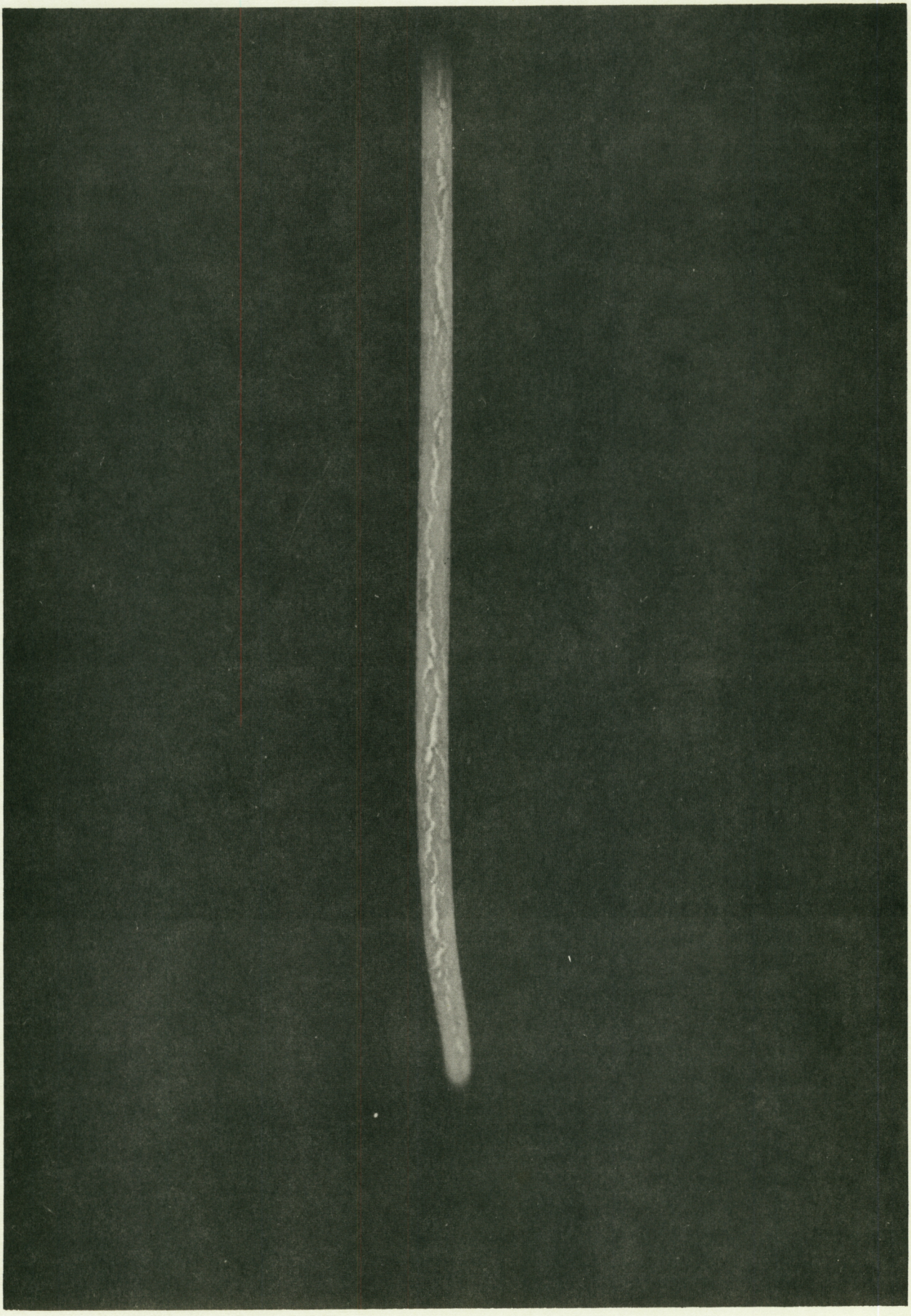

FIGURE 10

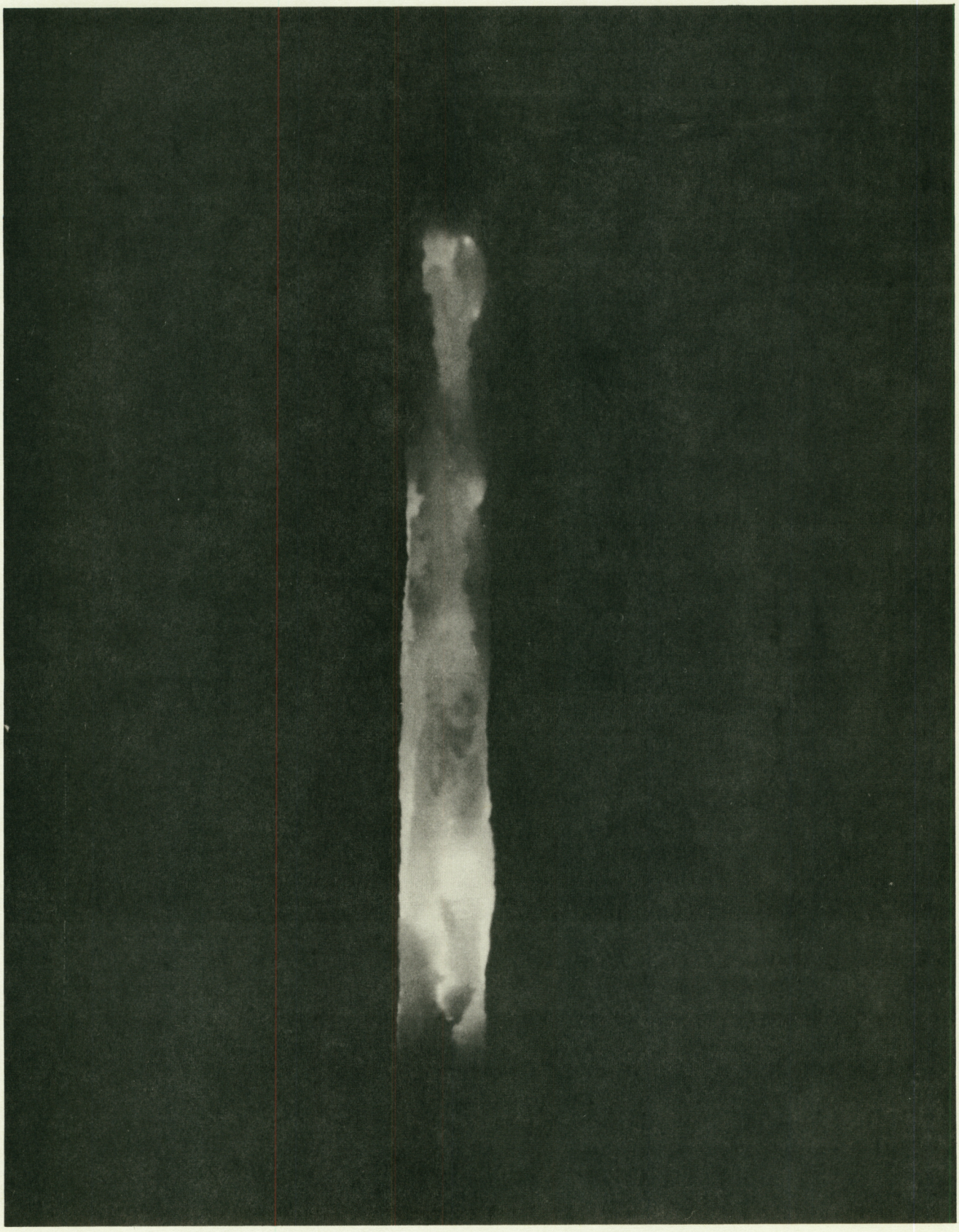

FIGURE 11

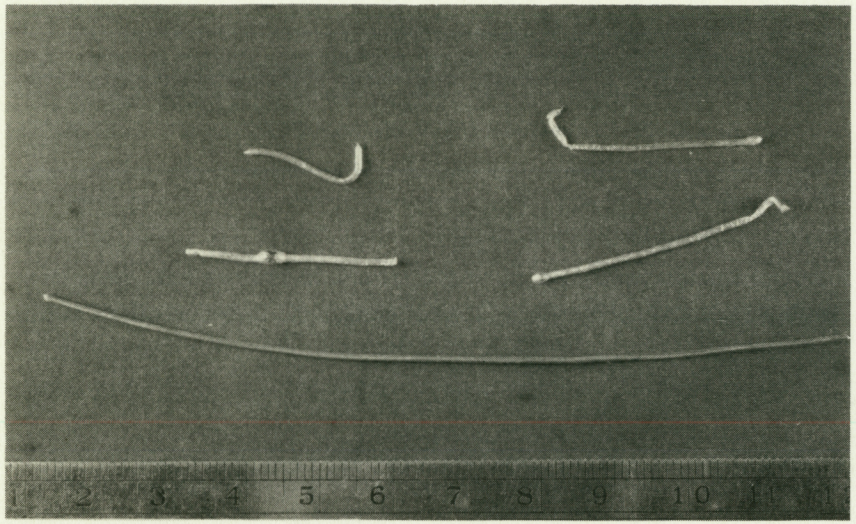

Al in $H_2O - O_2$

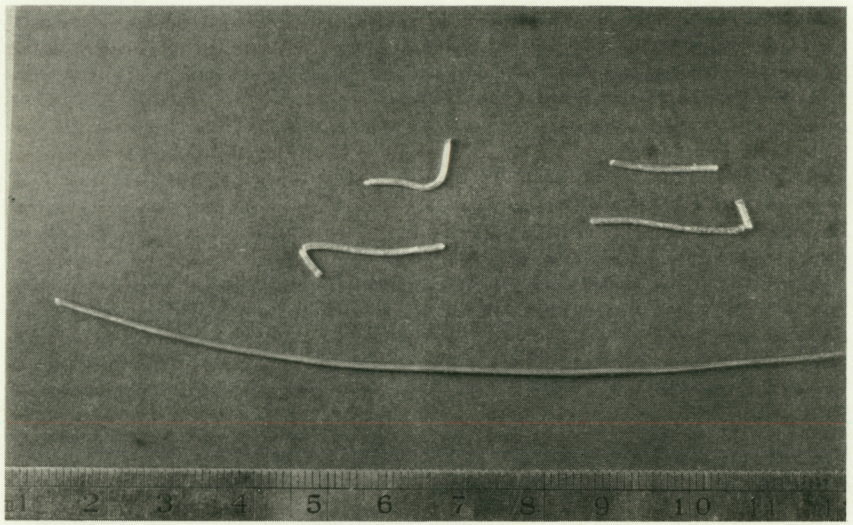

Al in $H_2O - CO_2$

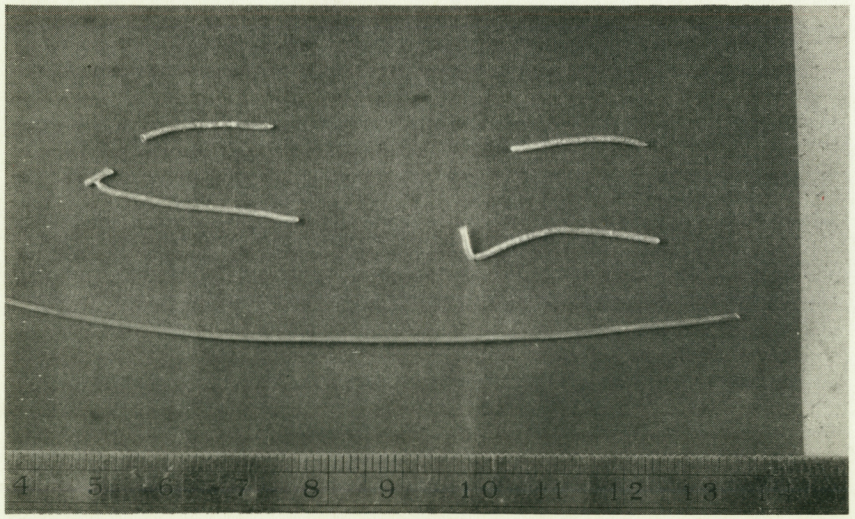

Al in H_2O - Ar

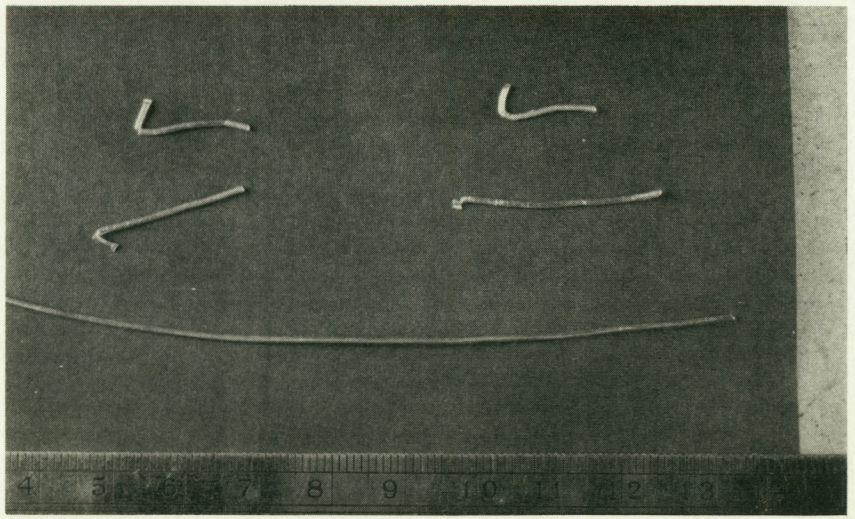

Al in Ar

FIGURE 12

RECOVERED REACTION PRODUCTS OF ALUMINUM WIRES HEATED IN $H_2O - O_2$, $H_2O - CO_2$, $H_2O - Ar$ & Ar; TOTAL PRESSURES 50 TO 200 mm Hg

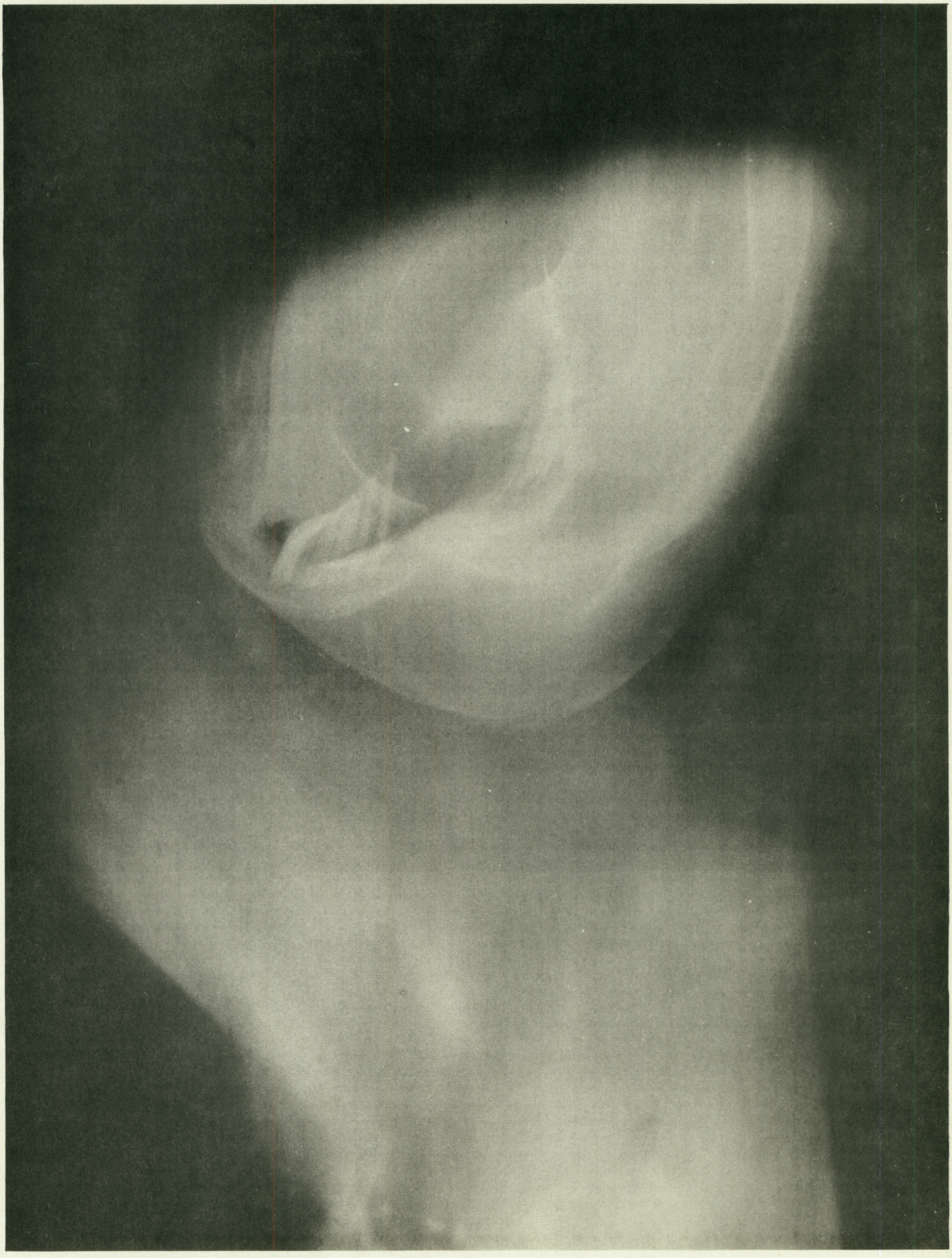

FIGURE 13

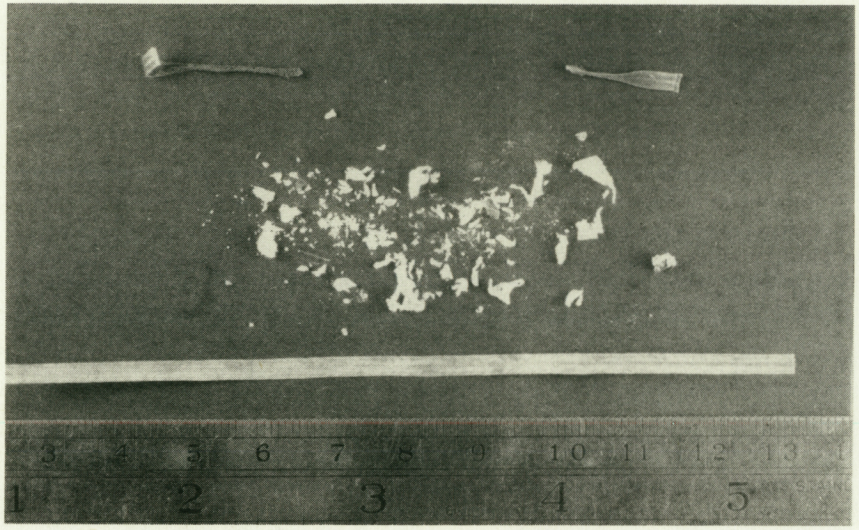

Mg in $H_2O - O_2$

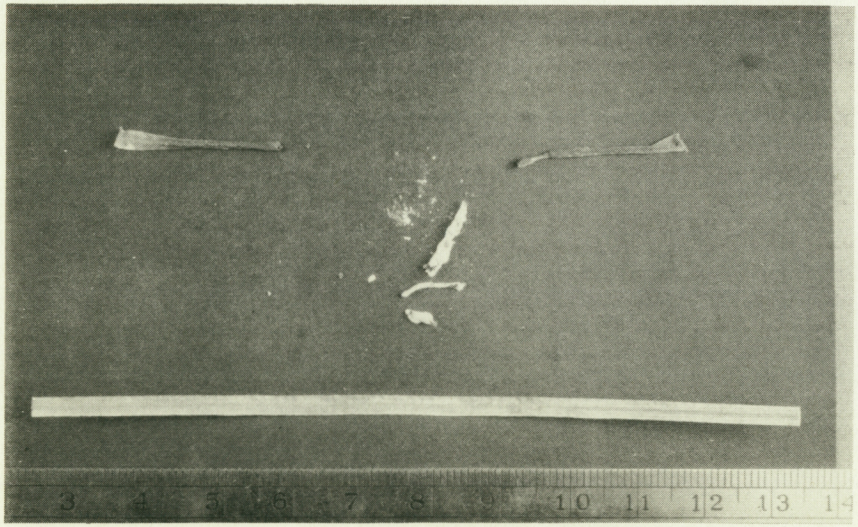

Mg in $H_2O - CO_2$

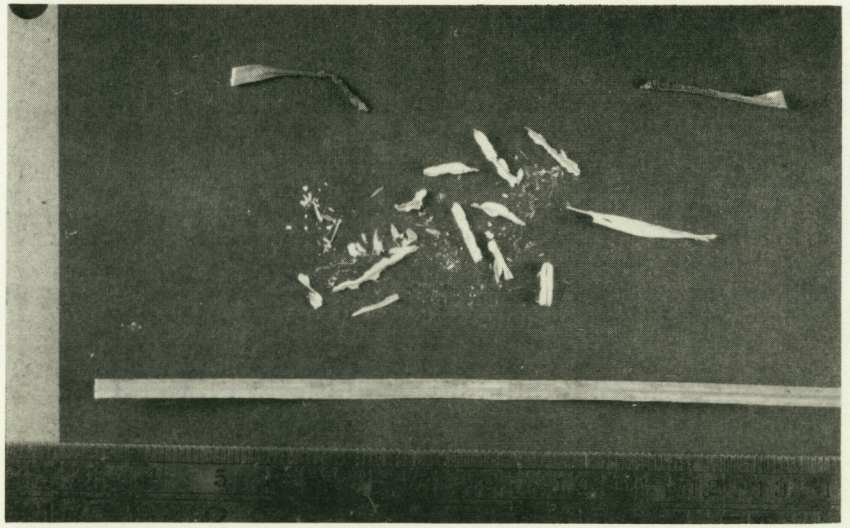

Mg in $H_2O - Ar$

FIGURE 14

RECOVERED COMBUSTION PRODUCTS OF MAGNESIUM RIBBONS HEATED IN $H_2O - O_2$, $H_2O - CO_2$, & $H_2O - Ar$; TOTAL PRESSURES 50 TO 200 mm Hg

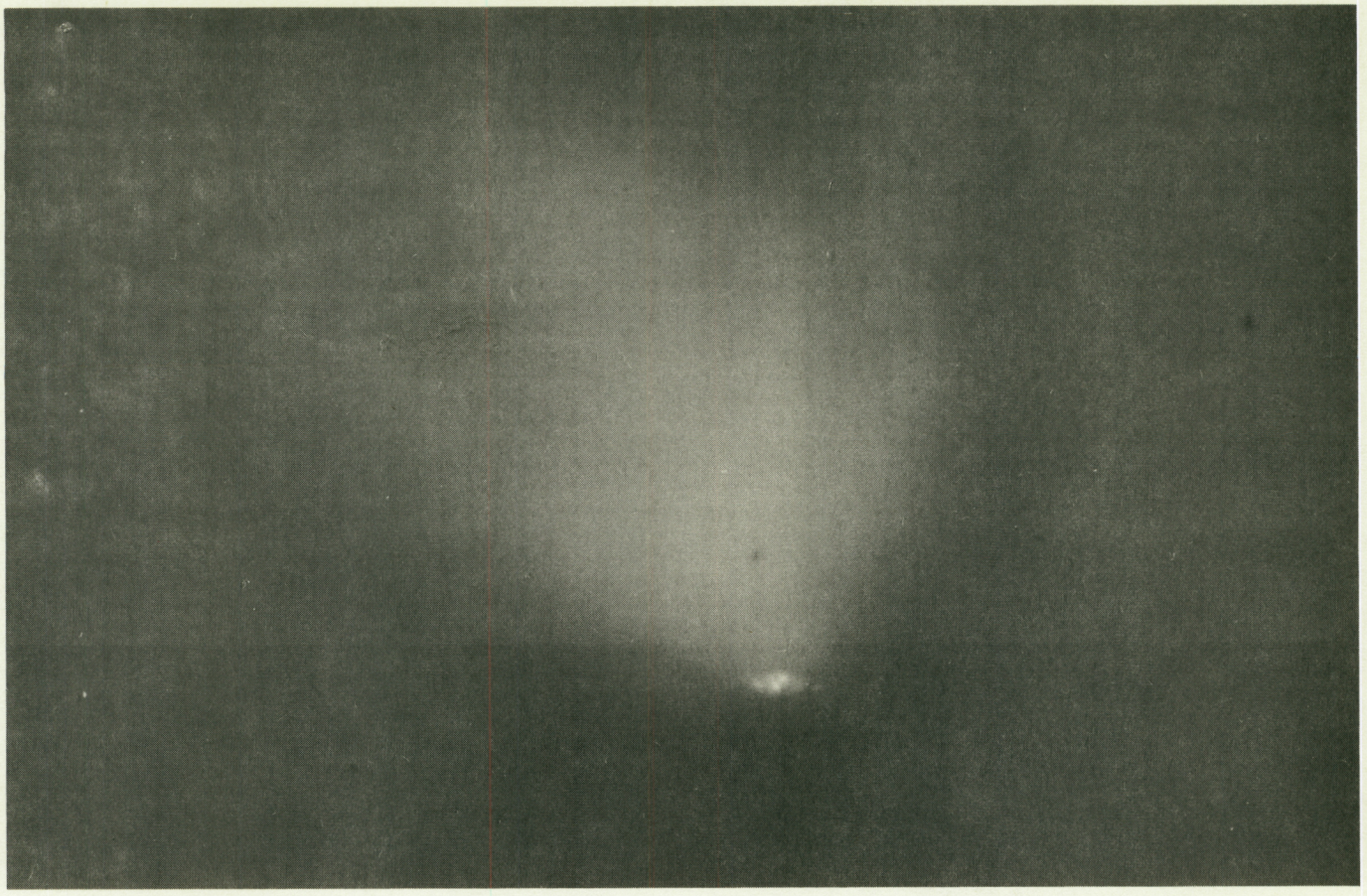

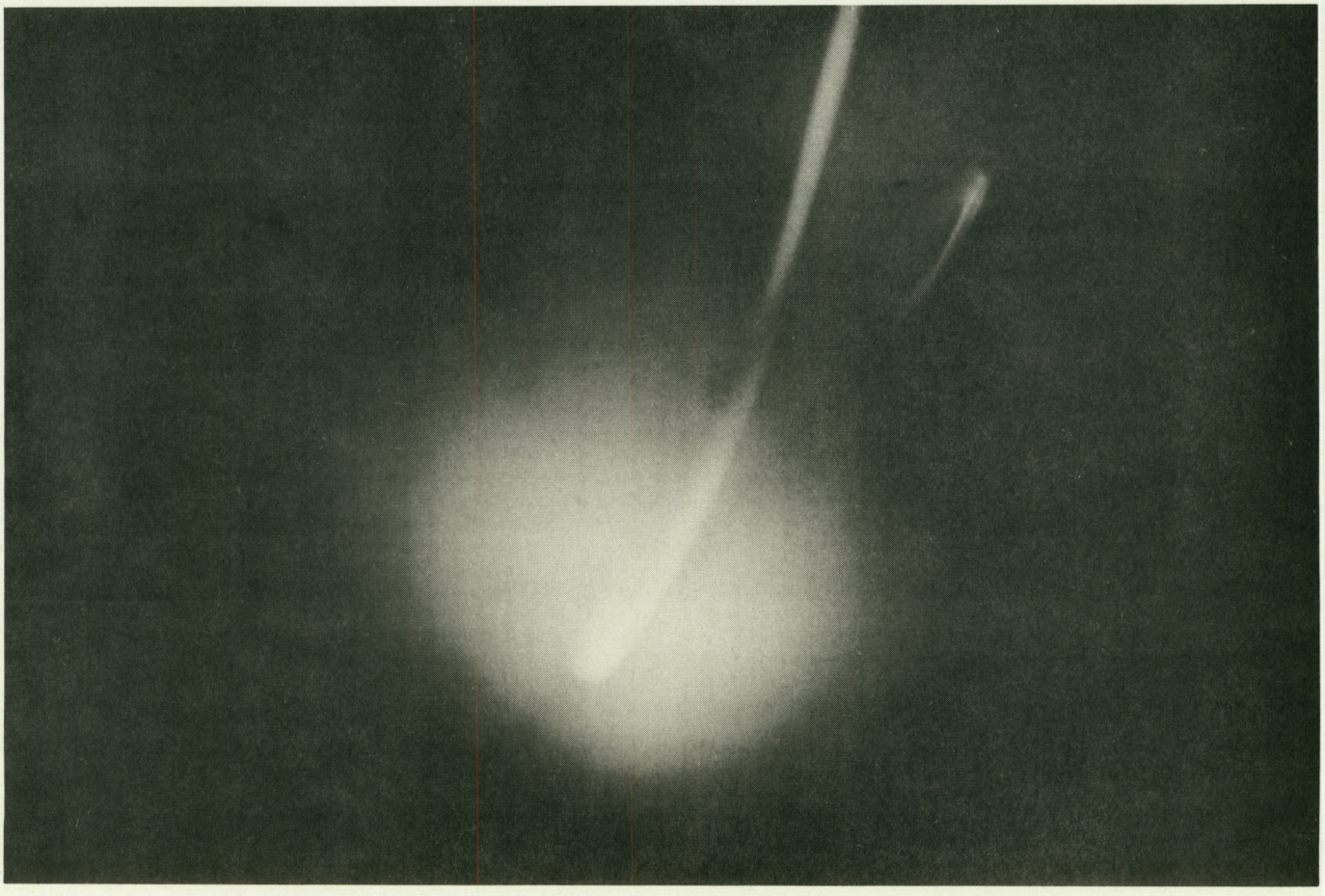

FIGURE 15

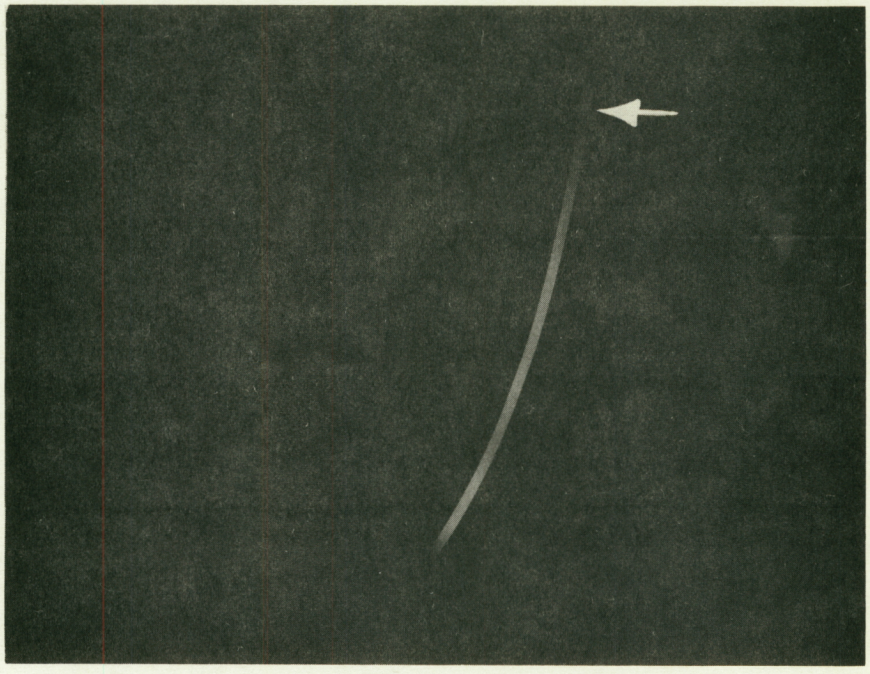

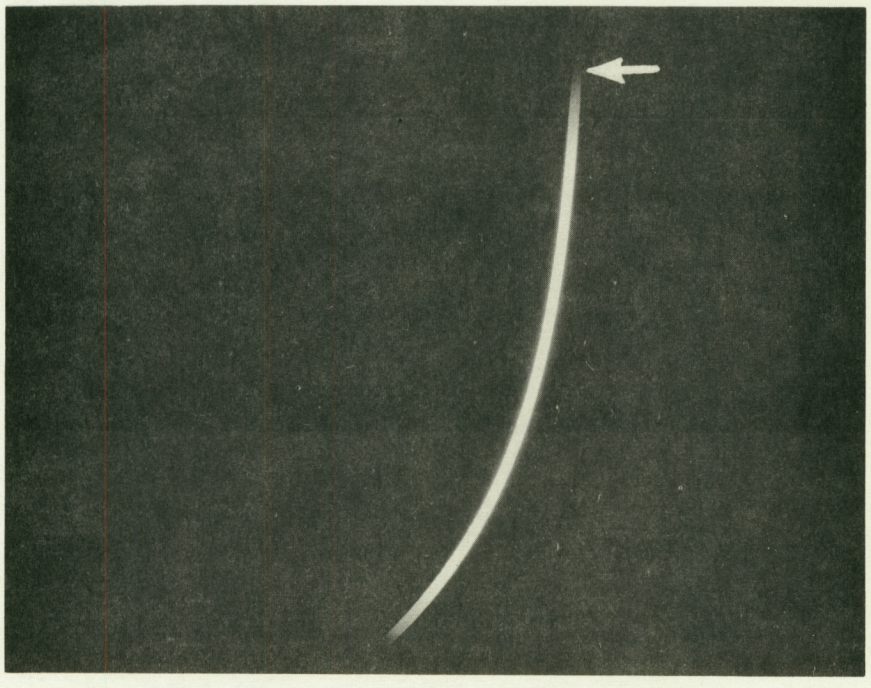

BRIGHT-DARK INTERFACE OBSERVED ON MOLYBDENUM WIRES HEATED IN PURE Ar AT 50 TORR

FIGURE 16

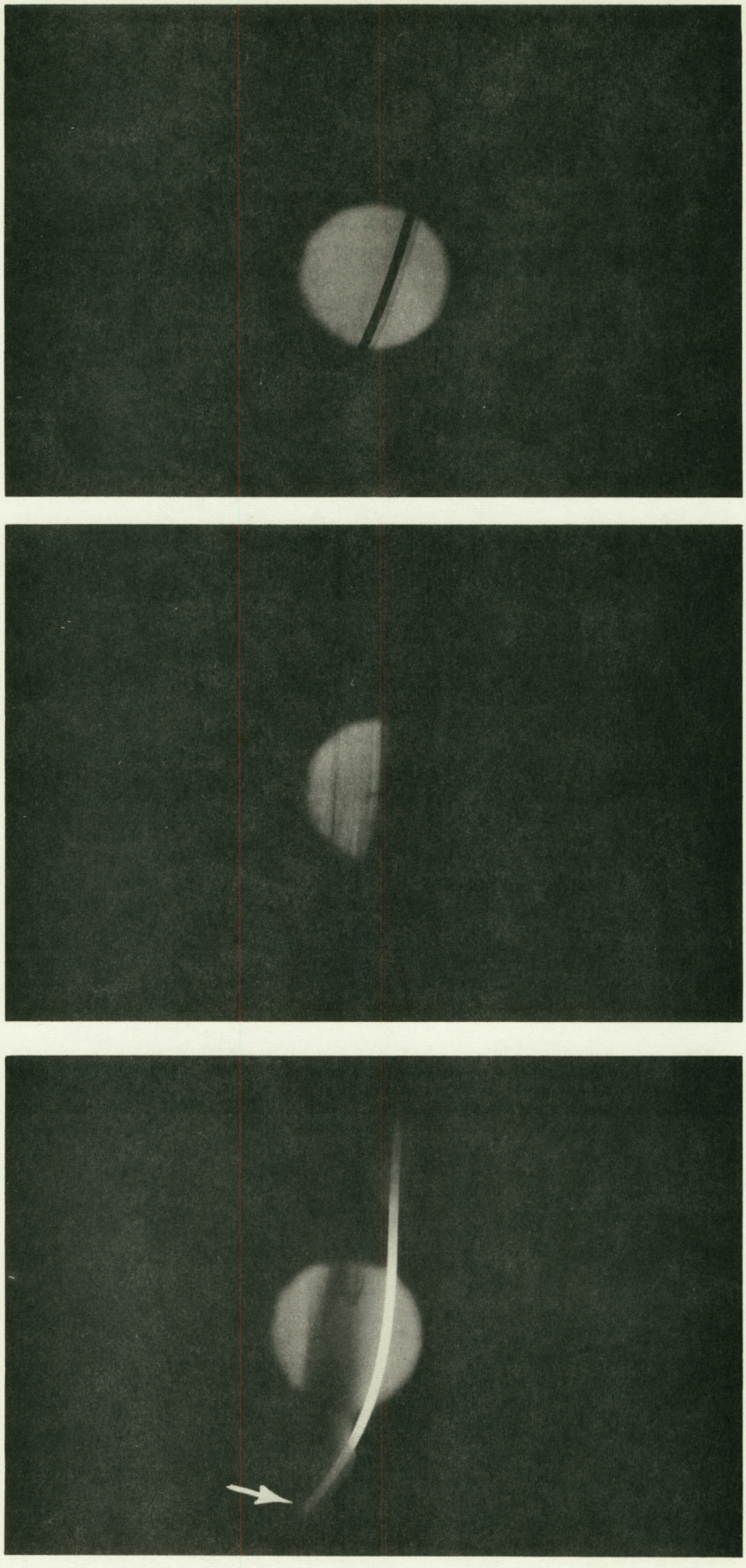

INCREASING TIME

PHOTOGRAPHS OF THE MOLYBDENUM CONDENSATION ZONE TAKEN WITH BACK ILLUMINATION AT 1ATM OF O_2

FIGURE 17

AP29-R-5-65

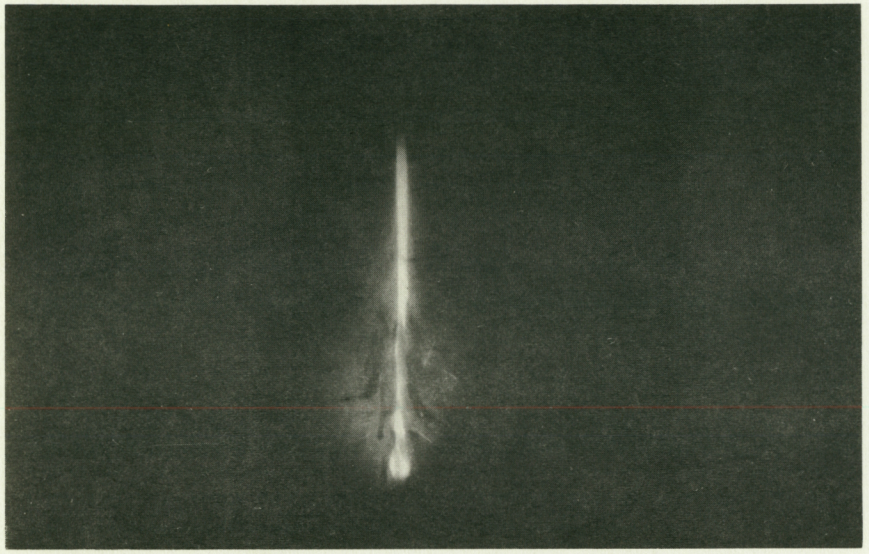

O_2 AT 2 ATM

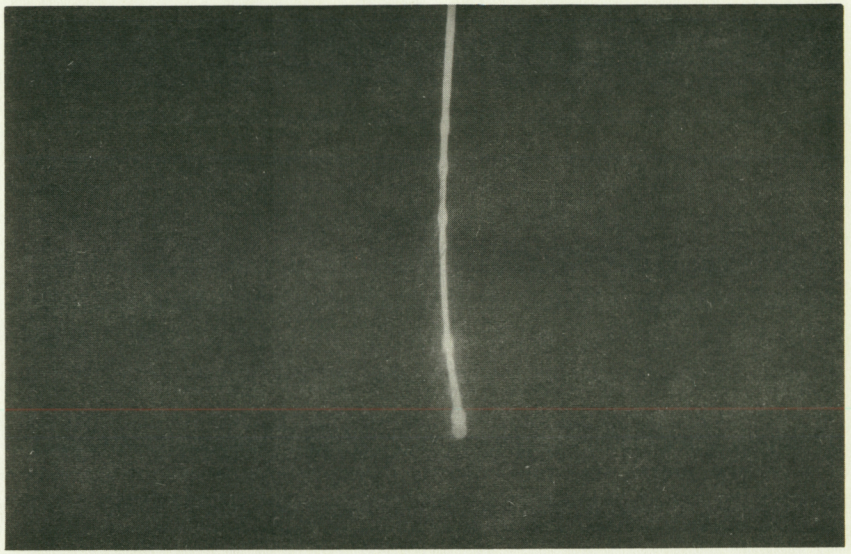

50% O_2 – 50% Ar AT 5 ATM

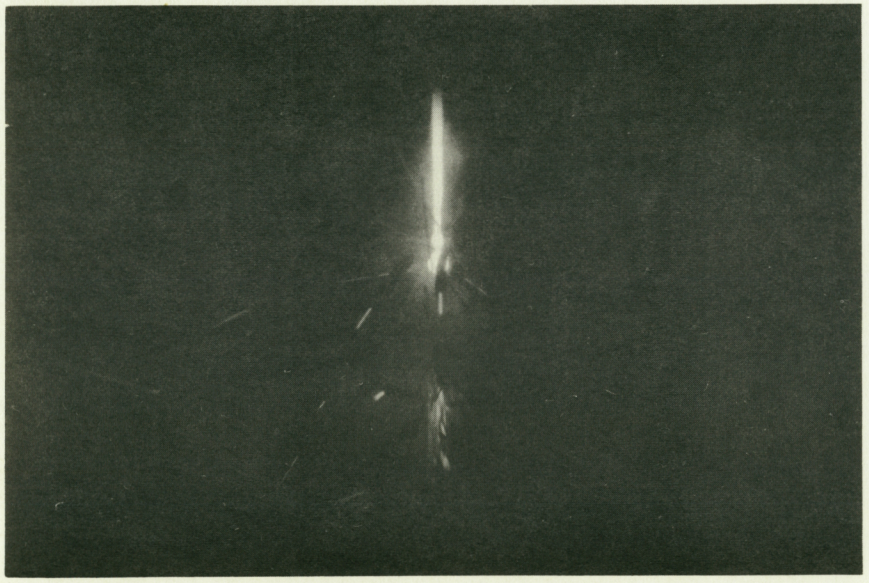

O_2 AT 5 ATM

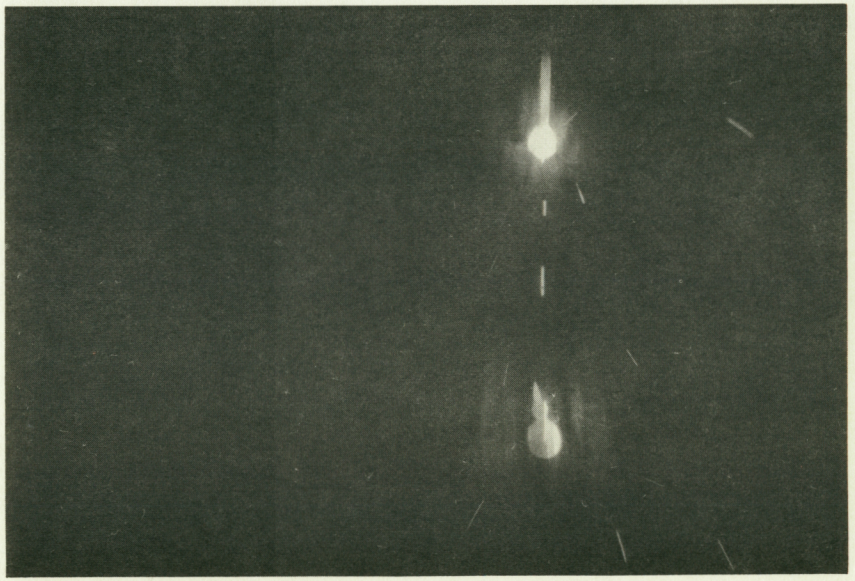

O_2 AT 500 TORR

FIGURE 18

REPRESENTATIVE SAMPLE PHOTOGRAPHS OF THE SOLID-PHASE COMBUSTION OF MOLYBDENUM IN REGIME ONE

JP29-P-8-65

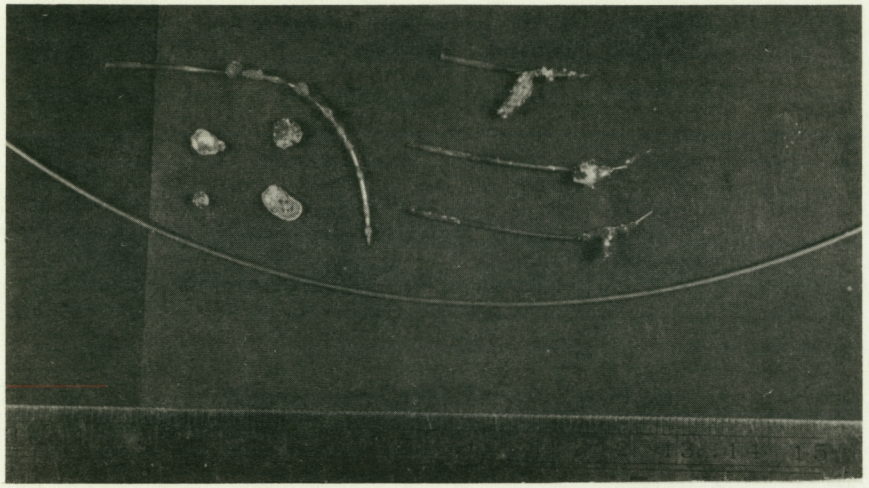

Mo IN REGIME ONE

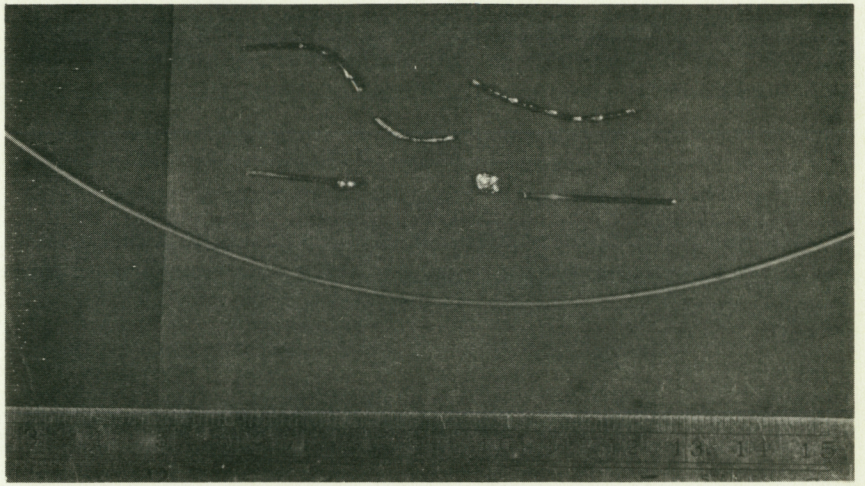

Mo IN REGIME TWO

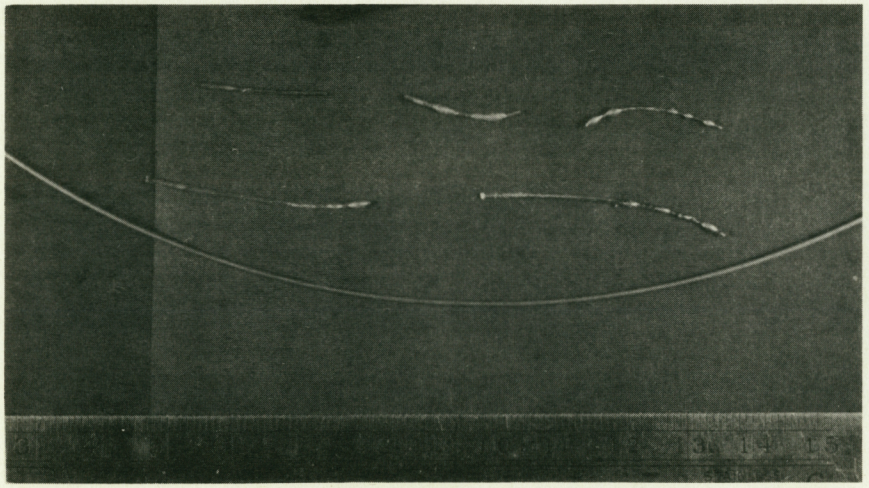

Mo IN REGIME THREE

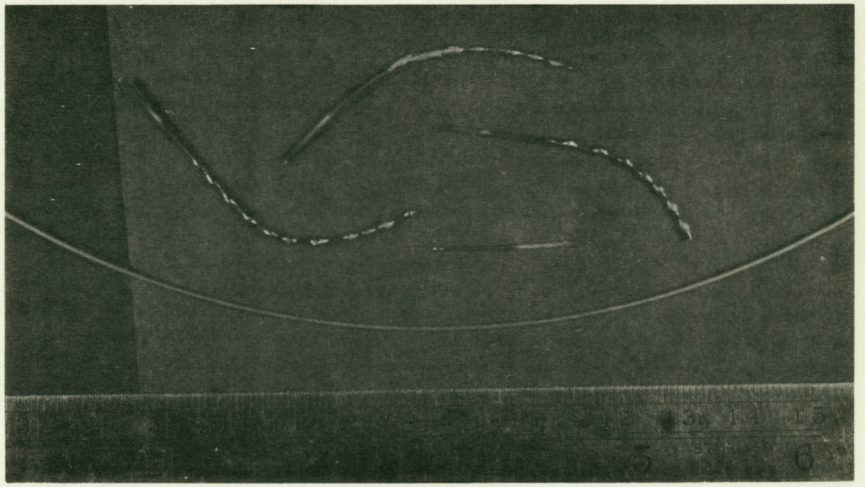

Mo IN REGIME FOUR

FIGURE 19

RECOVERED REACTION PRODUCTS OF MOLYBDENUM WIRES HEATED IN O_2-CO_2, O_2-Ar, & CO_2-Ar; TOTAL PRESSURES 50 TORR TO 5 ATM